SANDIA REPORT
SAND2003–2751
Unlimited Release
Printed August 2003

Thermal Analysis of Perforated Metal Air Transportable Package (PMATP) Prototype

Jim D. Pierce, John Mould, Howard Levine, and Robert Oneto

Prepared by
Sandia National Laboratories
Albuquerque, New Mexico 87185 and Livermore, California 94550

Sandia is a multiprogram laboratory operated by Sandia Corporation, a Lockheed Martin Company, for the United States Department of Energy's National Nuclear Security Administration under Contract DE-AC04-94AL85000.

Issued by Sandia National Laboratories, operated for the United States Department of Energy by Sandia Corporation.

Available to DOE and DOE contractors from
U.S. Department of Energy
Office of Scientific and Technical Information
P.O. Box 62
Oak Ridge, TN 37831

Telephone: (865) 576-8401
Facsimile: (865) 576-5728
E-Mail: reports@adonis.osti.gov
Online ordering: http://www.doe.gov/bridge

Available to the public from
U.S. Department of Commerce
National Technical Information Service
5285 Port Royal Rd.
Springfield, VA 22161

Telephone: (800) 553-6847
Facsimile: (703) 605-6900
E-Mail: orders@ntis.fedworld.gov
Online ordering: http://www.ntis.gov/help/ordermethods.asp?loc=7-4-0#online

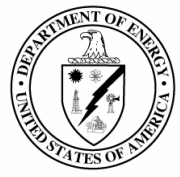

SAND2003-2751
Unlimited Release
Printed August 2003

Thermal Analysis of Perforated Metal Air Transportable Package (PMATP) Prototype

Jim D. Pierce
Dangerous Materials Mitigation and Disposition Department
Sandia National Laboratories
P.O. Box 5800
Albuquerque, NM 87185-0719

John Mould, Howard Levine, and Robert Oneto
Weidlinger Associates, Inc.
4410 El Camino Real, Suite 110
Los Altos, CA 94022

Prepared for Japan Nuclear Cycle Development Institute (JNC)

Abstract

Sandia National Laboratories (SNL) has designed a crash-resistant container, the Perforated Metal Air Transportable Package (PMATP), capable of surviving a worst-case plane crash, including both impact and subsequent fire, for the air transport of plutonium. This report presents thermal analyses of the full-scale PMATP in its undamaged (pre-test) condition and in bounding post-accident states. The goal of these thermal simulations was to evaluate the performance of the package in a worst-case post-crash fire. The full-scale package is approximately 1.6 m long by 0.8 m diameter. The thermal analyses were performed with the FLEX finite element code.

This analysis clearly predicts that the PMATP provides acceptable thermal response characteristics, both for the post-accident fire of a one-hour duration and the after-fire heat-soak condition. All predicted temperatures for the primary containment vessel are well within design limits for safety.

This work was supported by the Japan Nuclear Cycle Development Institute (JNC) under contract DE-F104-88AL5272, Appendix A-15, Statement of Work, and Section 1.2, Land Transport Emergency Response Technology.

Contents

Nomenclature **7**
1. Background and Scope **9**
2. Boundary and Initial Conditions **11**
3. Material Properties **13**
4. Infinite Cylinder Model **17**
5. Axisymmetric Model **19**
6. 3D Models **27**
7. 3D End-on Impact Model **29**
8. 3D Side-on Impact Model **33**
9. 3D Center-of-Gravity-Over-Corner Impact **37**
10. Summary and Conclusions **41**
11. References **43**

Figures

1. Perforated Metal Air Transportable Package (PMATP) 10
2a. Infinite Cylinder Model: Temperatures on Exterior Surface of PMATP 17
2b. Infinite Cylinder Model: Temperatures on Exterior Surface of the Primary Containment Vessel 18
3. Axisymmetric Finite-element Model of PMATP 20
4a. Finite-element Model and Steady-state Temperature [°C] Distribution from a 150-watt Internal Power Source 21
4b. Steady-state Temperature [°C] Distribution from the 150-watt Internal Power Source 22
5a. Finite-element Model and Temperature [°C] Distribution in PMATP at End of One-hour Fire 23
5b. Steady-state Temperature [°C] Distribution from a 150-watt Internal Power Source 24
6. Temperatures at the Exterior Surface and the Primary Containment Vessel 24
7a. Finite-element Model and Temperature [°C] Distribution in PMATP at Peak Temperature in the Primary Containment Vessel (20 hours) 25
7b. Temperature [°C] Distribution from a 150-watt Internal Power Source at Peak Primary Containment Vessel Temperature (20 hours) 26
8. 3D Finite-element Model of PMATP 27
9a. Comparison of 2D Axisymmetric and 3D Model Simulations at Outer Surface 28
9b. Comparison of 2D Axisymmetric and 3D Model Simulations at Primary Containment Vessel Surface 28
10a. Section View of One-half Scale PMATP after End-on Impact 30
10b. Finite-element Model of PMATP after End-on Impact 30
11. Temperature History at Center of Primary Containment Vessel After End-on Impact at Time 0 31
12. Temperature [°C] Distribution at End of Fire, End-on Impact 31

13. Temperature [°C] Distribution when Primary Containment Vessel is at its Peak Temperature (12 Hours After Start of Fire), End-on Impact 32
14a. Longitudinal Section of PMATP Following Side-on Impact 34
14b. Transverse Section of PMATP Following Side-on Impact 34
15. Sectioned Finite-element Model of PMATP Following Left Side (+x) Impact 35
16. Temperature Variation vs. Time at Center of Primary Containment Vessel 35
17. Temperature [°C] at End of Fire, Side-on Impact 36
18. Temperature [°C] Distribution when Primary Containment Vessel is at its Peak Temperature (12 Hours After Start of Fire), Side-on Impact 36
19. Cross Section of One-half Scale PMATP After CGOC Impact 38
20. Finite-element Model of PMATP Following CGOC Impact 38
21. Temperature Variation vs. Time at Primary Containment Vessel Centroid, CGOC Impact 39
22. Temperature [°C] at End of Fire, CGOC Impact 40
23. Temperature Distribution [°C] when Primary Containment Vessel is at its Peak Temperature (Approximately 22 Hours After Start of Fire), CGOC Impact 40
24. Time Variation of Temperature for the Undeformed and Deformed States of the PMATP at the Primary Containment Vessel Centroid 42

Tables

1. Temperature Dependence of Free Convection 11
2. 304L Stainless-steel Conductivity vs. Temperature 13
3. Specific Heat of Kevlar® 29 14
4. Homogenized Volume Ratio vs. Measured Crush 14
5. Heat Capacity ρC_p of Homogenized Overpack [J/°C-m^3] 15
6. In-plane Conductivity of Homogenized Overpack [W/m-°C] 15
7. Through-plane Conductivity of Homogenized Overpack [W/m °C] 16

This page intentionally left blank.

Nomenclature

2D	two-dimensional
3D	three-dimensional
CGOC	center-of-gravity-over-corner
PMATP	Perforated Metal Air Transportable Package
SNL	Sandia National Laboratories

This page intentionally left blank.

1. Background and Scope

Sandia National Laboratories (SNL) has designed a crash resistant container capable of surviving a worst-case plane crash, including both impact and subsequent fire, for the air transport of plutonium.[1] As shown in Figure 1, the Perforated Metal Air Transportable Package (PMATP) consists of a substantial stainless steel primary containment vessel within an overpack of layered perforated aluminum and Aramid cloth, surrounded by a thinner stainless steel shell.

As part of design evaluation, SNL has conducted extensive analytical studies, laboratory tests on the component materials, and field impact tests on one-half scale models.

This report presents the results of thermal analyses of the full-scale package in both its undamaged (pre-test) condition, and in bounding post-accident states for side-on impact, end-on impact, and center-of-gravity-over-corner (CGOC) impact. The full-scale package is approximately 1.6 m long by 0.8 m diameter. The goal of these thermal simulations was to evaluate the performance of the package in a post-crash fire. The thermal analyses were performed with the FLEX finite element code.[2]

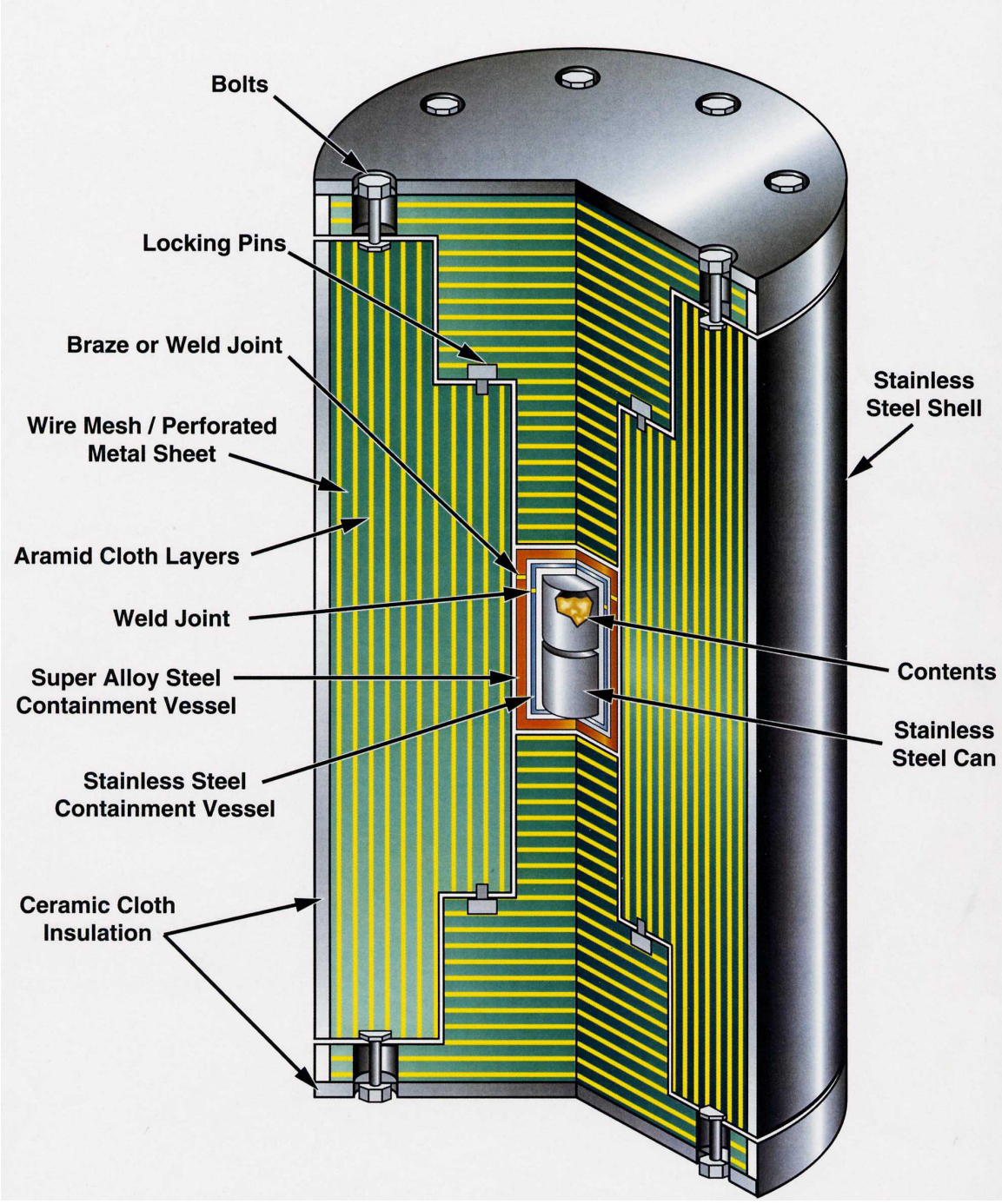

Figure 1. Perforated Metal Air Transportable Package (PMATP).

2. Boundary and Initial Conditions

Ambient air temperature is assumed to be 37.8°C. The internal package heating as a result of the plutonium radiation is represented as a 150-watt continuous power source. The initial temperature distribution within the PMATP was computed as the steady-state distribution in an undamaged package heated by the plutonium, with radiation and free convection into 37.8°C air.

According to NUREG-0360,[3] the most severe likely fire environment can be simulated by a black-body radiation source at 1,010°C for a duration of one hour. The maximum temperatures at interior points may occur well after the fire is finished, so the simulation extends until the internal temperatures have peaked and are declining. During the cooling phase, radiation and free convection into the ambient environment were considered. In determining the convection coefficients, the horizontal position of the package was assumed.

For radiation heat transfer, the flux per unit area is calculated as:

$$\dot{q} = \sigma E \left(T^4 - T_0^4 \right)$$

Here, T denotes the absolute surface temperature, T_0 the fire/ambient air temperature, E the emissivity of the package (E = 0.8), and σ, the Stefan-Boltzmann constant [5.67×10^{-8} W/(m^2 K^4)].

The heat flux per unit area during free convection is calculated as shown by Todd and Ellis:[4]

$$\dot{q} = h\left(T - T_0 \right)^n$$

Here, the exponent n is equal to 1.333 for both the end plates and the horizontal cylinder surfaces. The heat transfer coefficient, *h*, is a function of average temperature: $T_{avg} = 0.5(T + T_0)$. The values of *h* were almost the same for the end plates and horizontal cylindrical surface, so *h* was calculated for ambient temperature and in 100°C increments to beyond the regulating 1000°C fire, and the average values are shown in Table 1.

Table 1. Temperature Dependence of Free Convection

T_{avg} [°C]	*h*[W/(°C^n m^2)]
–73.15	1.872
26.85	1.398
126.85	1.18
226.85	1.018
326.85	0.905
426.85	0.815
526.85	0.746
626.85	0.690
726.85	0.641
826.85	0.605
926.85	0.572
1026.85	0.545
1126.85	0.522

This page intentionally left blank.

3. Material Properties

Available thermophysical properties were used for all of the constituent materials in the package. For values outside the temperature range of the data, bounding values were used. Phase changes caused by melting of metals or charring of Kevlar®* were not considered.

The S304L stainless steel is modeled as an isotropic material with conductivity varying with temperature as shown in Table 2. Handbook values[4] based on approximate alloy percentages are presented.

Density = 8030 [kg/m^3]
Specific heat = 460 [J/kg-°C]

Table 2. 304L Stainless-steel Conductivity vs. Temperature

Temperature [°C]	Conductivity [W/m-°C]
0	16.3
100	17
200	17
300	19
400	19
600	22
800	27
1000	31

The S138 stainless steel was modeled using constant properties because it was not exposed to severe temperature variations.

Density = 7800 [kg/m^3]
Specific heat = 460 [J/kg-°C]
Conductivity = 17 [W/m-°C]

The steel pellets used as a plutonium simulant were also modeled using constant properties because the temperatures are expected to be nearly constant. These properties are based on the volume fractions of air and steel.

Density = 4085 [kg/m^3]
Specific heat = 721 [J/kg-°C]
Conductivity = 8.53 [W/m-°C]

* Kevlar® is a DuPont registered trademark.

The overpack consists of layers of perforated 3003 aluminum and Kevlar® 29 cloth, fabric style 710. Kevlar® properties are given by Lopez and Pierce[5] as:

Density = 794.91 [kg/m^3]
Conductivity = 0.081 [W/m-K]
The specific heat of Kevlar® 29 variation with temperature is given in Table 3.

Table 3. Specific Heat of Kevlar® 29

Temperature [°C]	Specific Heat [J/kg-K]
23	1135
50	1210
100	1355
200	1596
300	1849
400	2105

Perforated aluminum properties are also given by Lopez and Pierce[5] for a range of temperatures and experimental crush. Crush is the height of a perforated aluminum sample after crushing relative to its initial height. Note that the oiled rather than the cleaned material properties discussed in Lopez and Pierce[5] were used where available because the actual packages will likely be constructed from oiled rather than cleaned material.

There were too many layers to model each explicitly in a three-dimensional (3D) simulation; consequently, a homogenized overpack material model was constructed. For each crush value, the aluminum volume ratio = V^A/V_0^A was calculated based on the reported densities. Assuming that all volume change occurs in the aluminum, and none in the Kevlar®, a homogenized volume ratio equal to V/V_0 was obtained corresponding to each crush value. These values are tabulated in Table 4. Note it is these homogenized volume ratios that must be correlated with the observed dimensions of crushed scale models.

Table 4. Homogenized Volume Ratio vs. Measured Crush

Crush [%]	V/V_0
0	1.0
20	0.839
35	0.740
40	0.704
45	0.669
50	0.633

For each value of temperature and crush, we calculate the homogenized heat capacity as:

$$\rho^H C^H = \left(\rho^A C^A \frac{V^A}{V} + \rho^K C^K \frac{V^K}{V} \right),$$

The homogenized in-plane conductivity is based on parallel heat flow:

$$K^H = \frac{K^K V^K + K^A V^A}{V}$$

The homogenized through-plane conductivity is based on series heat flow:

$$K^H = \frac{V}{\frac{V^A}{K^A} + \frac{V^K}{K^K}}$$

These values are given in Tables 5 through 7.

Table 5. Heat Capacity ρC_p of Homogenized Overpack [J/°C-m^3]

	Crush [%]					
Temperature °C	0	20	35	40	45	48.5
23	1067087	1272452	1532723	1633302	1700992	1779999
50	1091951	1302101	1568436	1671358	1740626	1821473
100	1136972	1355787	1633103	1740269	1812393	1896574
200	1205948	1438038	1732178	1845845	1922344	2011632
300	1275683	1521193	1832341	1952582	2033504	2127955
400	1349830	1609610	1938844	2066073	2151699	2251640
500	1403495	1673603	2015926	2148214	2237243	2341158

Table 6. In-plane Conductivity of Homogenized Overpack [W/m-°C]

	Crush [%]					
Temperature °C	0	20	35	40	45	48.5
23	2.382225	4.895829	11.0894	13.07681	14.07513	17.21449
50	2.439473	5.213295	11.40198	13.28759	14.22444	17.33651
100	2.54549	5.801195	11.98083	13.67791	14.50094	17.56247
200	2.667939	6.527049	12.42654	14.02372	14.78481	17.84085
300	2.774061	6.729976	12.57511	14.12391	14.85577	17.91044
400	2.89651	6.948513	12.42654	13.88791	14.5719	17.70166
500	2.953653	7.049976	12.35226	13.72464	14.359	17.21449

Table 7. Through-plane Conductivity of Homogenized Overpack [W/m °C]

	Crush [%]					
Temperature °C	0	20	35	40	45	48.5
23	0.2953486	0.3308824	0.3021451	0.2893774	0.2749375	0.2641937
50	0.3053077	0.3333143	0.3023655	0.2893774	0.2749375	0.2642035
100	0.3225224	0.3351339	0.3025784	0.2892108	0.2749375	0.2642324
200	0.3315104	0.3376329	0.3027843	0.2888236	0.27458	0.2642789
300	0.3358609	0.3393813	0.3031762	0.2889569	0.2744338	0.2642698
400	0.339879	0.3413826	0.3033628	0.288997	0.2744338	0.2642698
500	0.341775	0.341876	0.3031762	0.2894581	0.2743177	0.2641737

4. Infinite Cylinder Model

To evaluate the level of approximation in homogenizing the layered material, the PMATP was simulated as an infinite cylinder. Figures 2a and 2b compare temperatures at the outer surface of the container and the outer surface of the primary containment vessel for an explicit model (i.e., each layer of Kevlar® and each layer of perforated aluminum modeled explicitly), a homogenized model using the fine explicit mesh, and a homogenized model using a coarser mesh at a resolution comparable to that to be used in the 3D models.

For these comparisons, temperature independent values of specific heat and conductivity were assumed for each material. The internal power deposition per unit length was equivalent to a 100-watt source in the full-scale package.

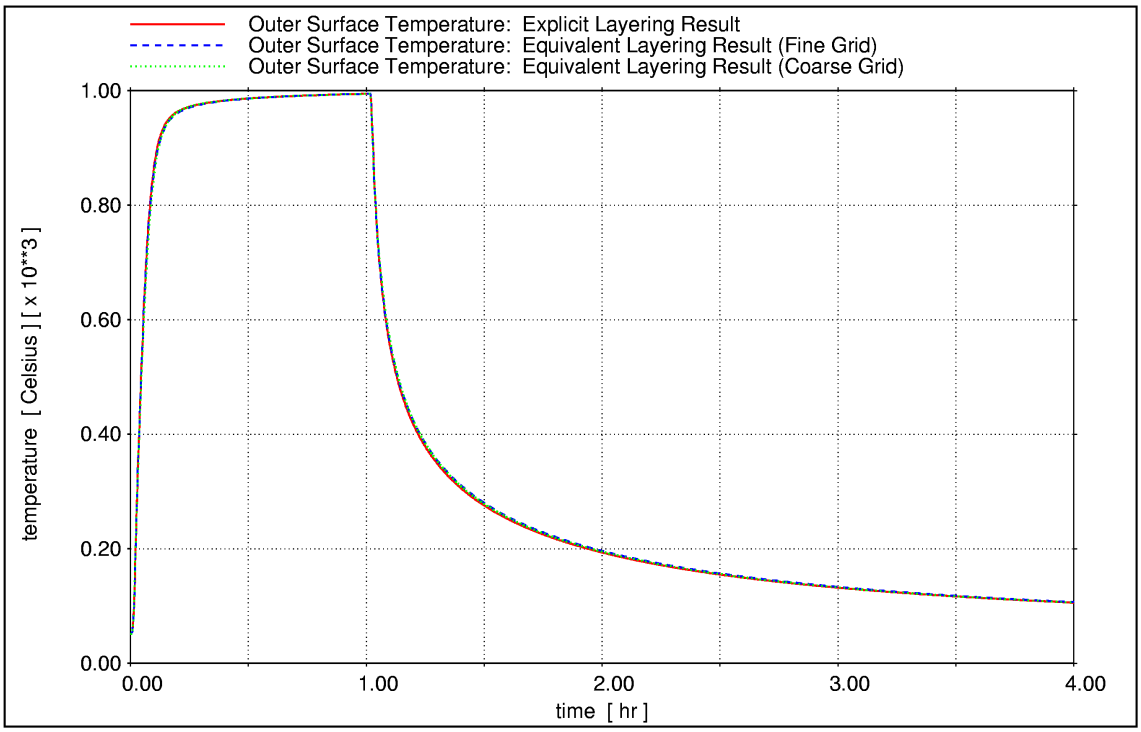

Figure 2a. Infinite Cylinder Model: Temperatures on Exterior Surface of PMATP.

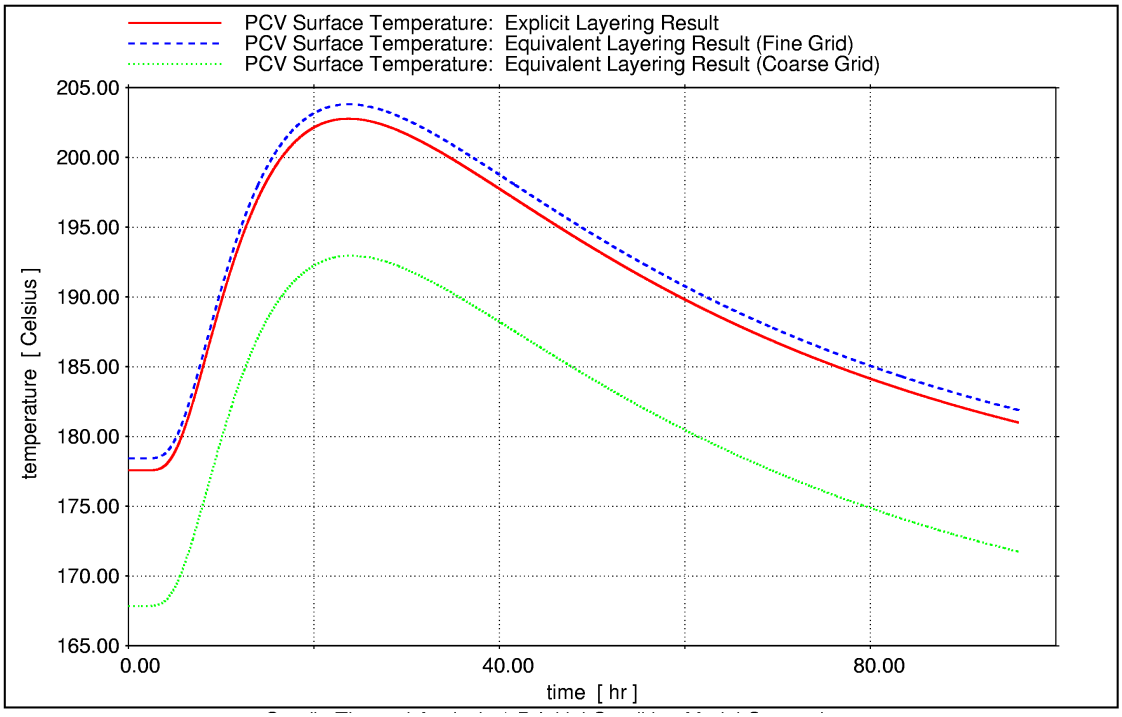

Figure 2b. Infinite Cylinder Model: Temperatures on Exterior Surface of the Primary Containment Vessel.

From this comparison, we conclude that homogenization of the material properties has negligible effect on the solution. The coarser grid calculation underestimates the peak temperature at the primary containment vessel by approximately 10 degrees Celsius.

5. Axisymmetric Model

Figure 3 shows a two-dimensional (2D) axisymmetric finite element model of the package. The four-character material designations are acronyms for the actual materials. ASTL refers to the air/steel-pellet plutonium simulant, WPAK is the homogenized wrapped packing material and SPAK designates the homogenized stacked packing material at the ends. In addition, S138 refers to the super-alloy steel containment vessel, and S304 is the stainless steel containment vessel.

Figure 4a depicts the steady-state temperature distribution induced by a 150-watt internal power source. Temperature profiles along axial and radial lines through the centroid of the primary containment vessel are shown in Figure 4b. This calculation included radiation and free convection into 37.8°C air on the outside wall.

Figure 5a shows the temperature distribution throughout the package at the end of a one-hour fire. Profiles along axial and radial lines through the centroid of the primary containment vessel are shown in Figure 5b.

Figure 6 shows the variation of temperature with time at the outer surface and at the primary containment vessel. As expected, the peak surface temperature of 1000°C occurred during the fire; however, the peak temperature at the primary containment vessel occurred much later – approximately 20 hours after the beginning of the fire. Figure 7a shows the temperature distribution at this time. Figure 7b shows the axial and radial profiles. Figure 6 also shows that the primary containment vessel increased to approximately 175°C, resulting in a difference of only 30°C from steady state to the peak temperature as a result of this accident fire simulation.

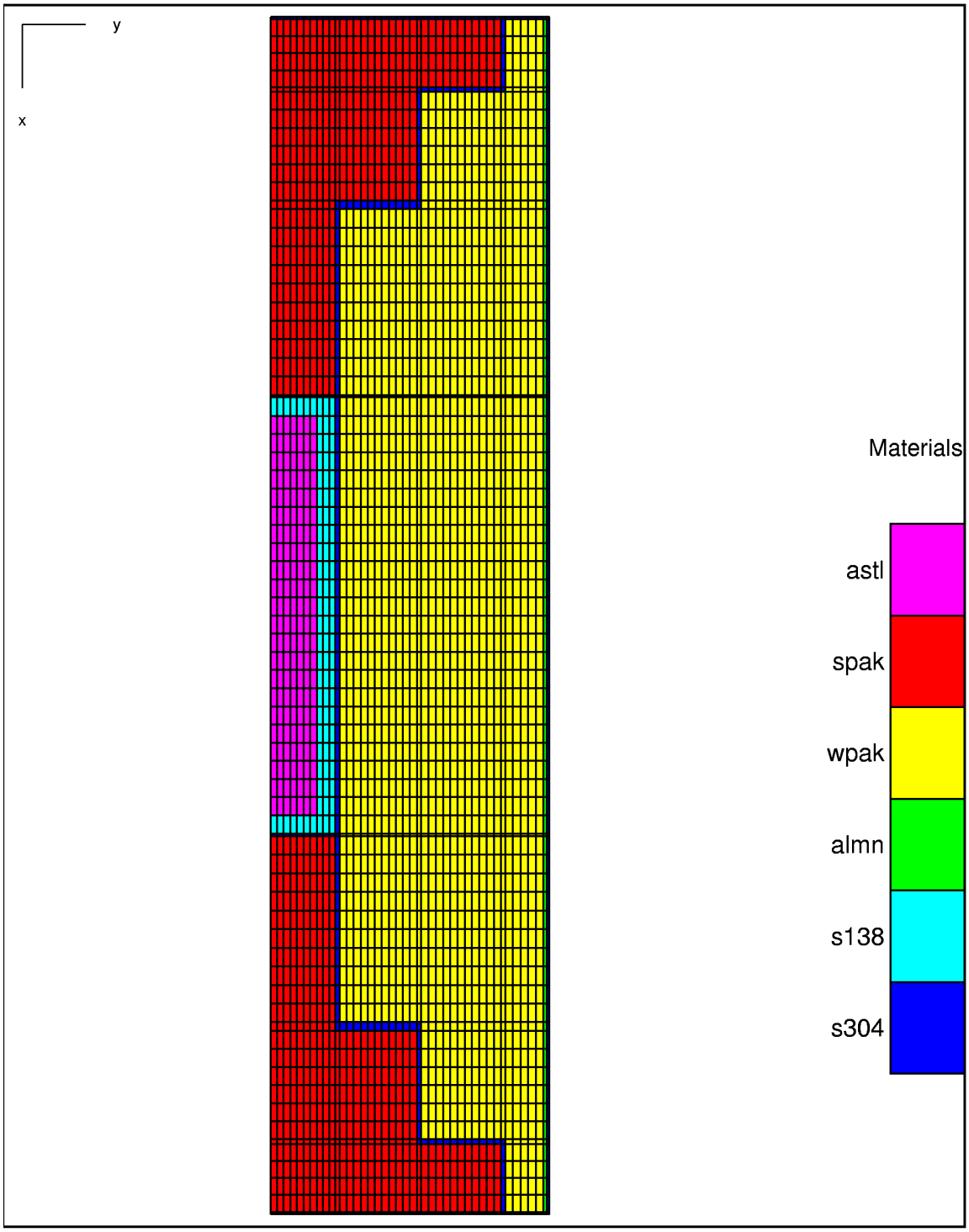

Figure 3. Axisymmetric Finite-element Model of PMATP.

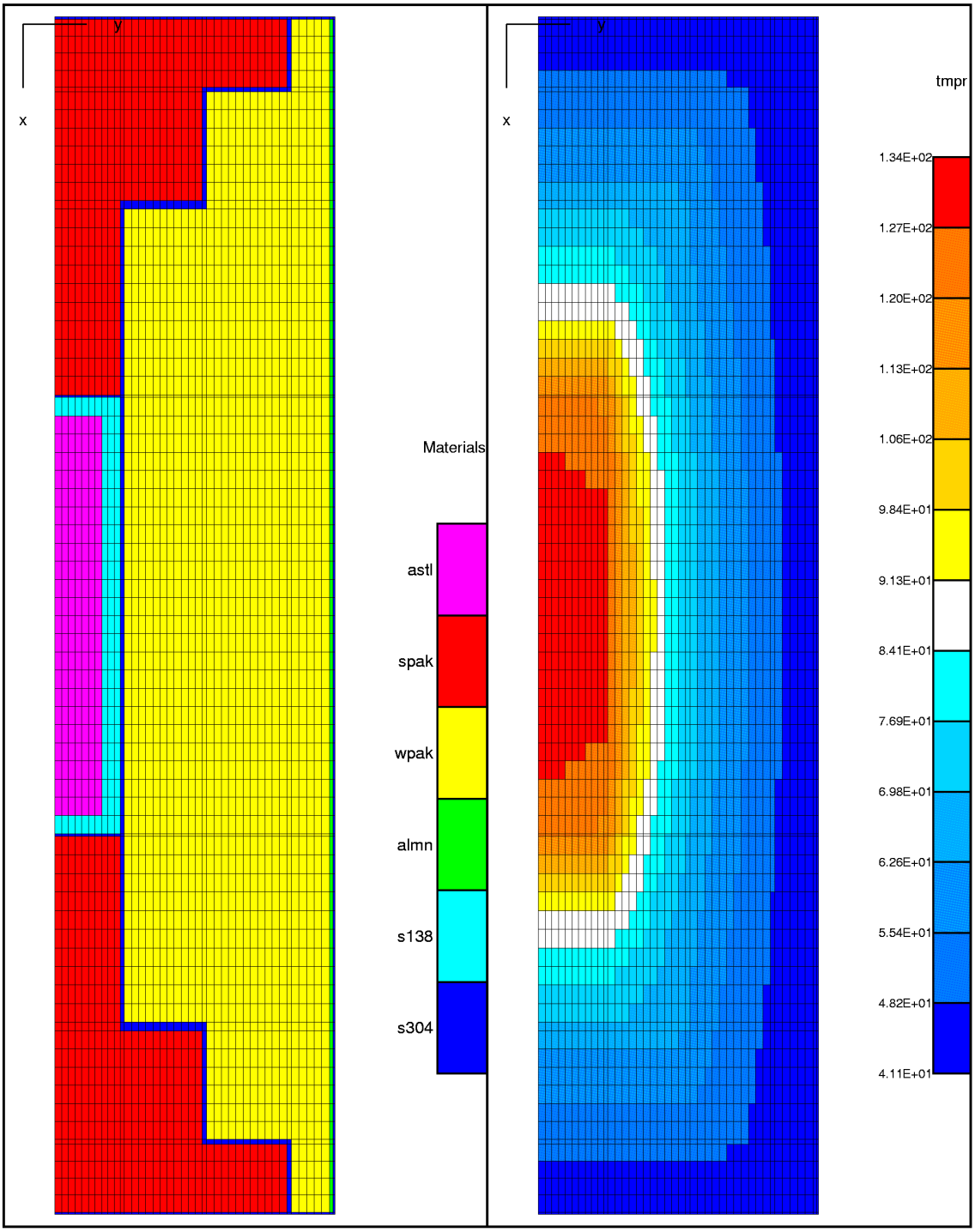

Figure 4a. Finite-element Model and Steady-state Temperature [°C] Distribution from a 150-watt Internal Power Source.

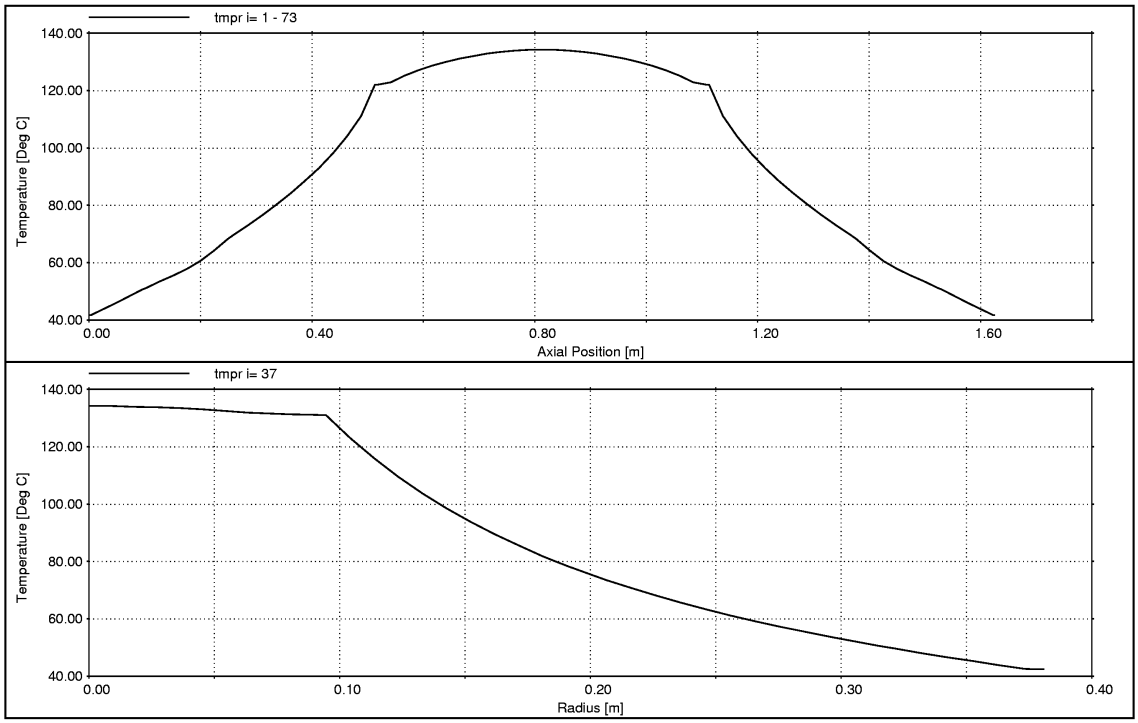

Figure 4b. Steady-state Temperature [°C] Distribution from the 150-watt Internal Power Source. Axial and radial sections are through the centroid of the primary containment vessel.

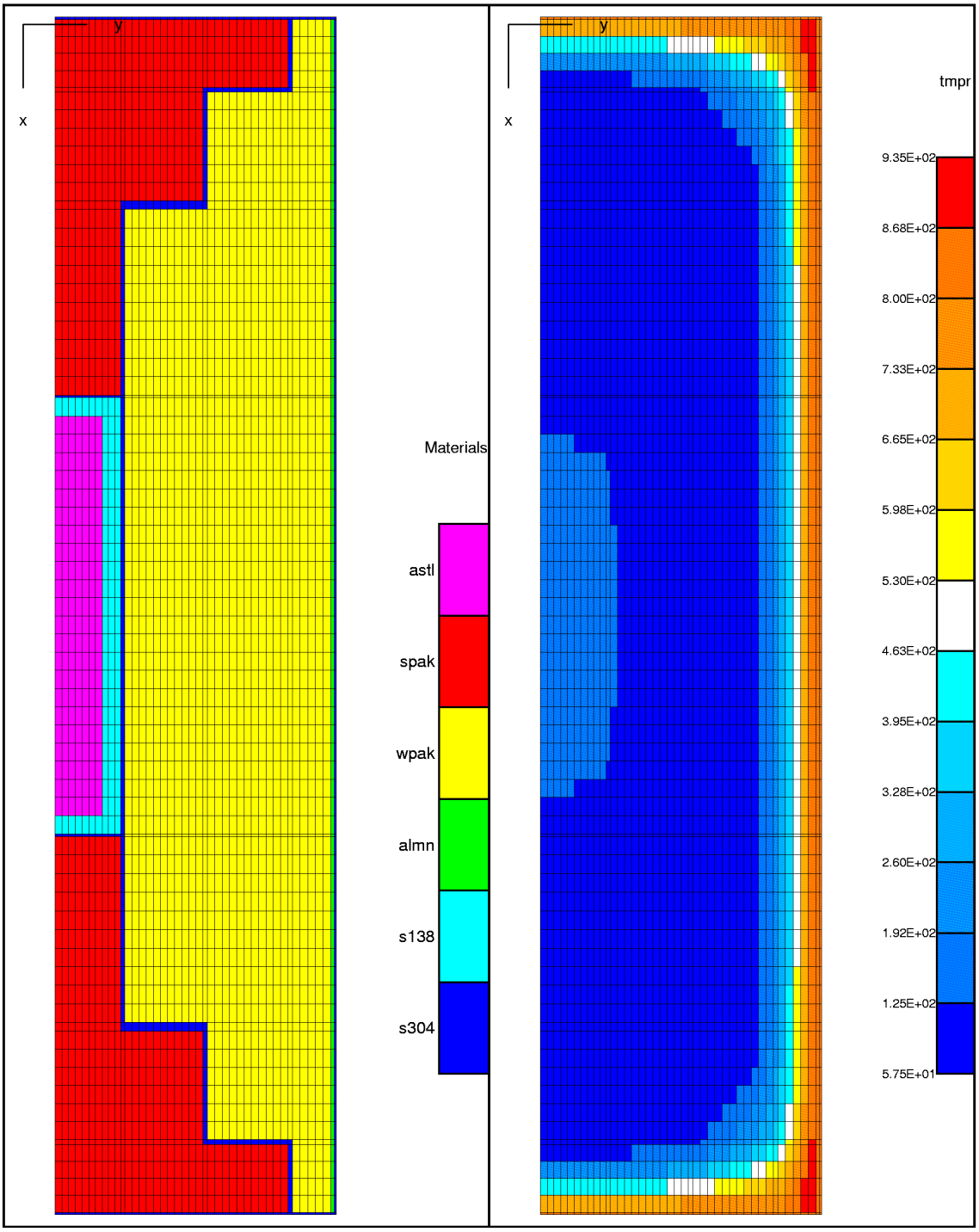

Figure 5a. Finite-element Model and Temperature [°C] Distribution in PMATP at End of One-hour Fire.

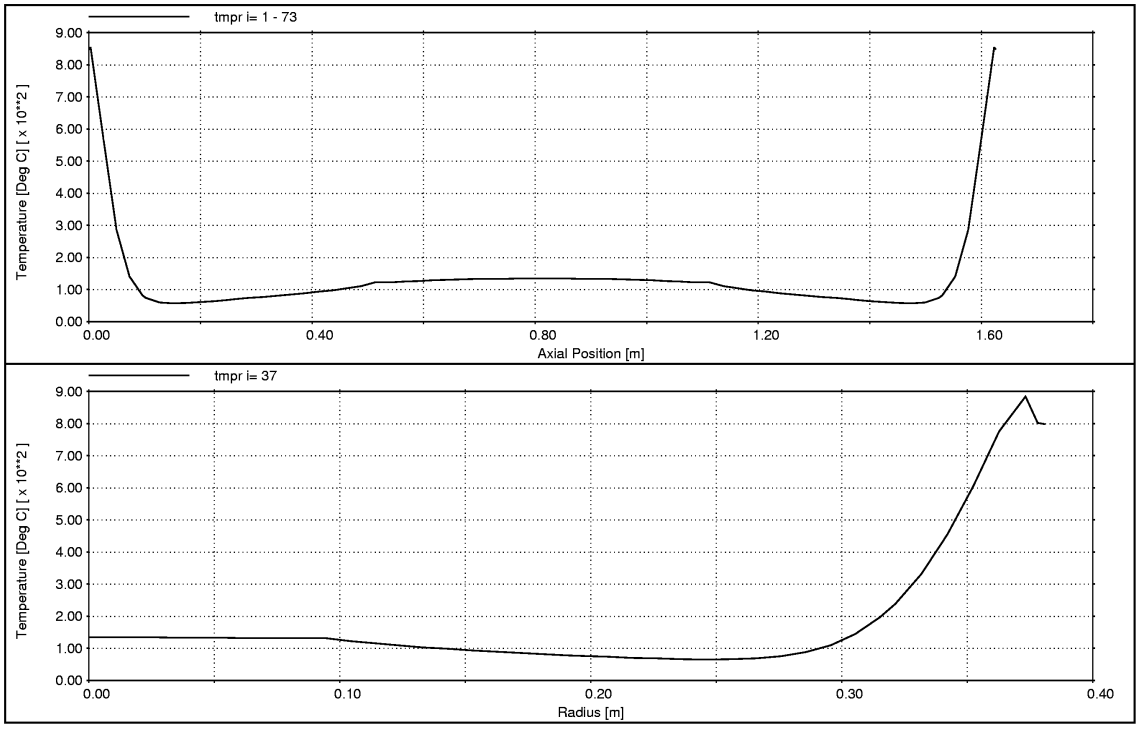

Figure 5b. Steady-state Temperature [°C] Distribution from a 150-watt Internal Power Source. Axial and radial sections are through the centroid of the primary containment vessel.

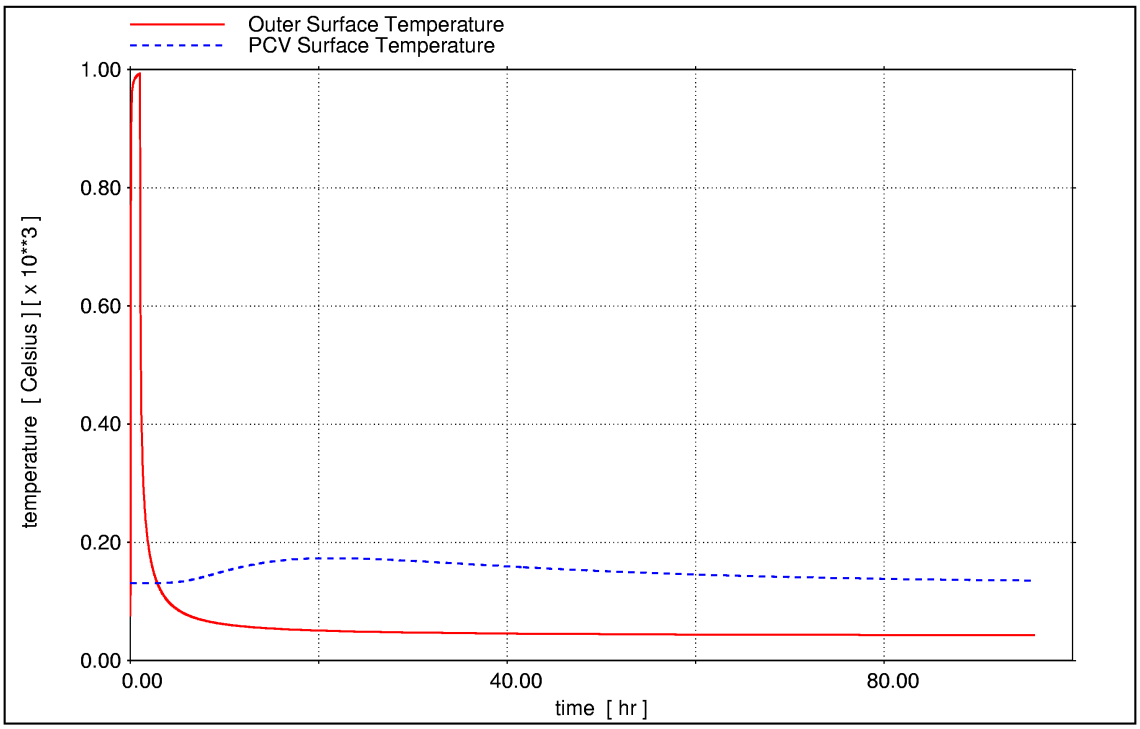

Figure 6. Temperatures at the Exterior Surface and the Primary Containment Vessel.

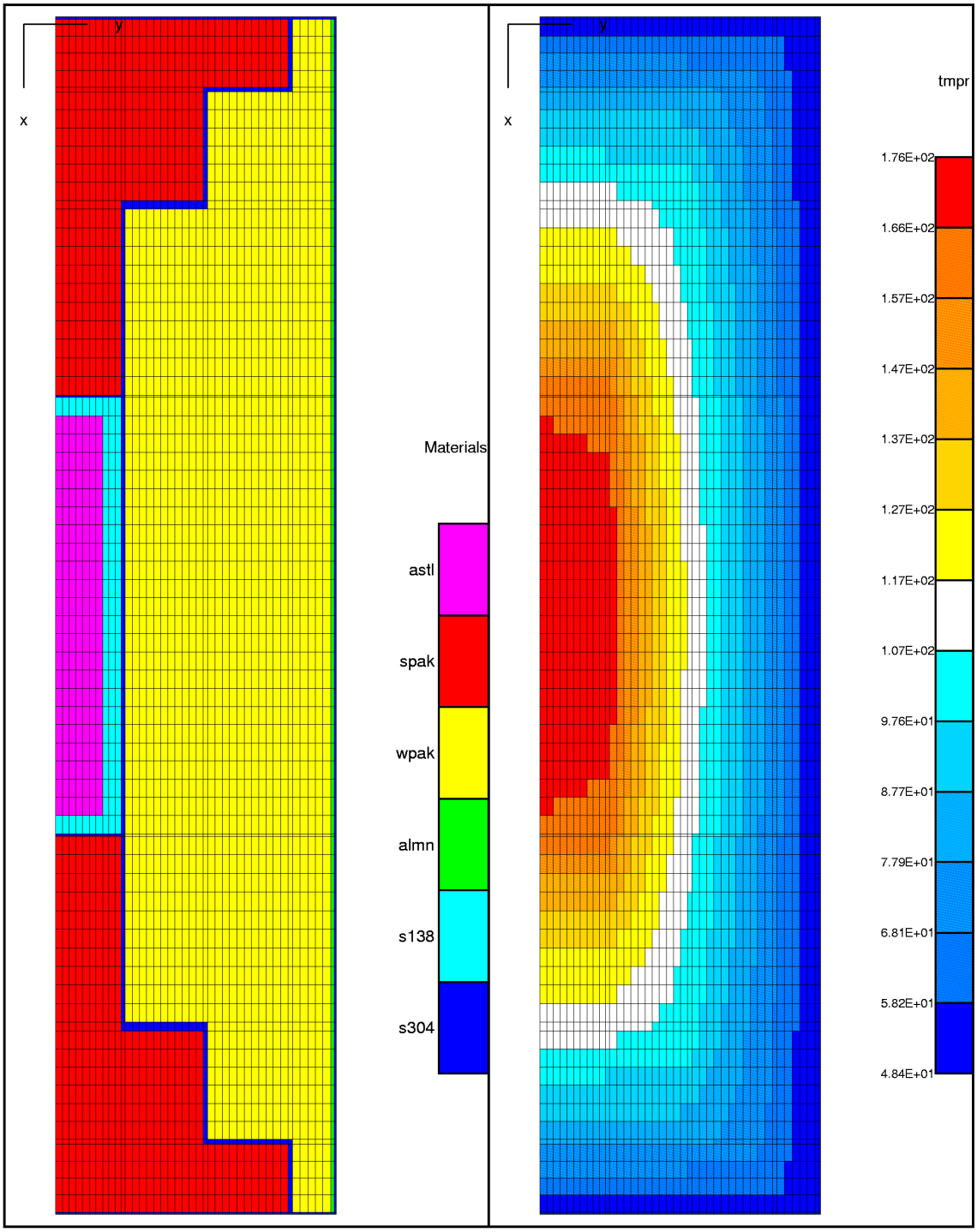

Figure 7a. Finite-element Model and Temperature [°C] Distribution in PMATP at Peak Temperature in the Primary Containment Vessel (20 hours).

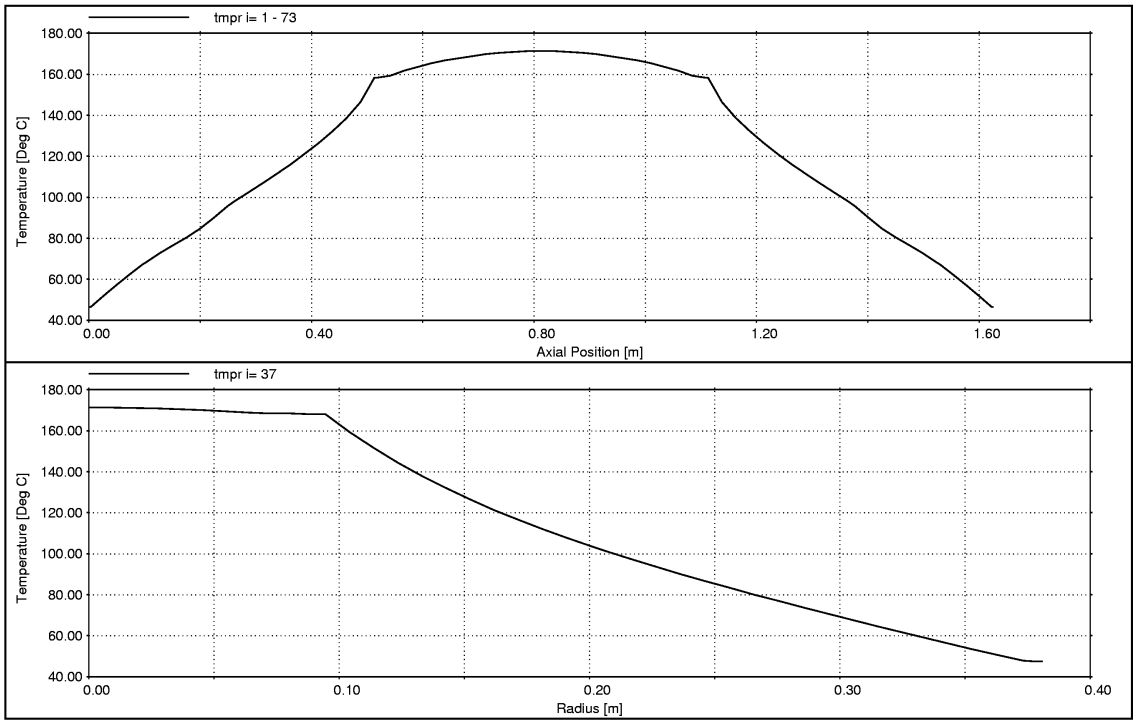

Figure 7b. Temperature [°C] Distribution from a 150-watt Internal Power Source at Peak Primary Containment Vessel Temperature (20 hours). Axial and radial sections are through centroid of the primary containment vessel.

6. 3D Models

Figure 8 shows a three-dimensional (3D) finite-element model of the PMATP. In Figures 9a and 9b, temperatures calculated with this model are compared to the two-dimensional (2D) axi-symmetric results as a consistency check. They agree very well. Distorted versions of this model corresponding to end-on, side-on and center-of-gravity-over-corner (CGOC) impacts were also calculated to provide post-impact thermal analysis. There were small design/fabrication differences between these three one-half scale test articles – especially in the end caps. The analyses described in this report assume a common design based on drawings for the CGOC test article.

The distorted models were produced by deforming the initial model to match post-impact test photographs of the one-half-scale impact specimens. Key points on the photographs were identified and correlated with the corresponding points on the undeformed model. These points were moved to their geometrically similar, post-impact positions. Tri-linear interpolation was used to define the positions of grid nodes between the key points. Volume ratios and layer orientations were also assigned based on the photographs. At the end of this process, the deformed geometry and volume ratio (or strain) fields were available for the thermal analysis.

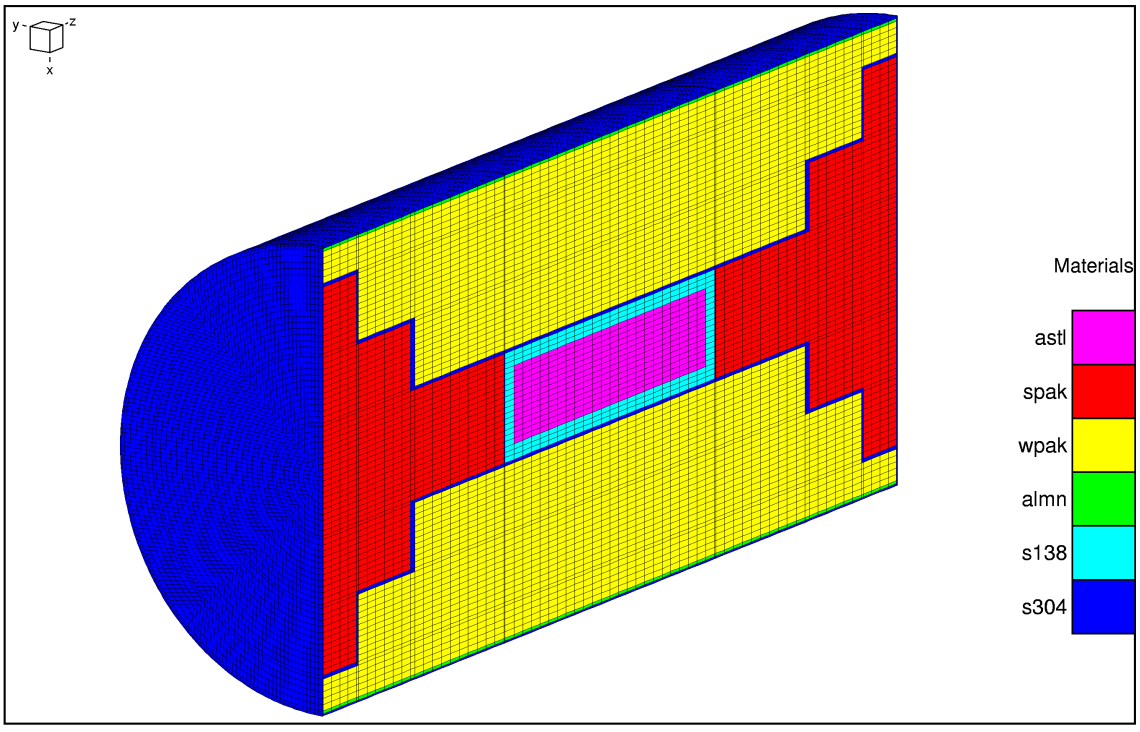

Figure 8. 3D Finite-element Model of PMATP.

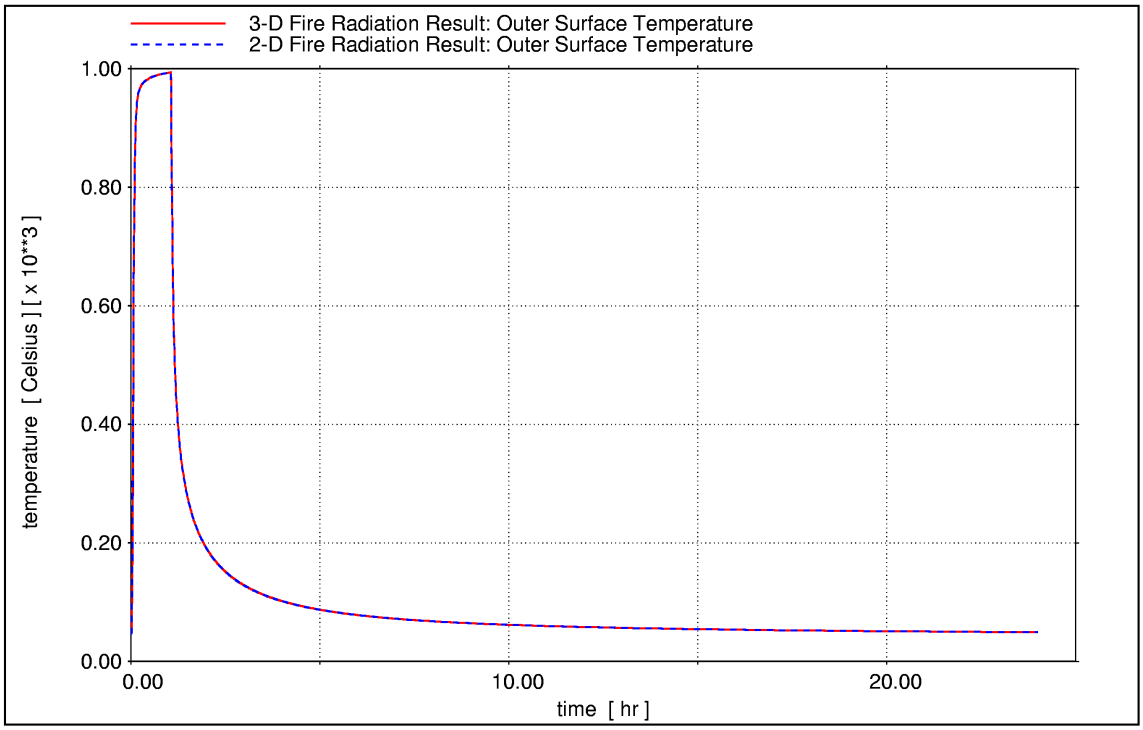

Figure 9a. Comparison of 2D Axisymmetric and 3D Model Simulations at Outer Surface.

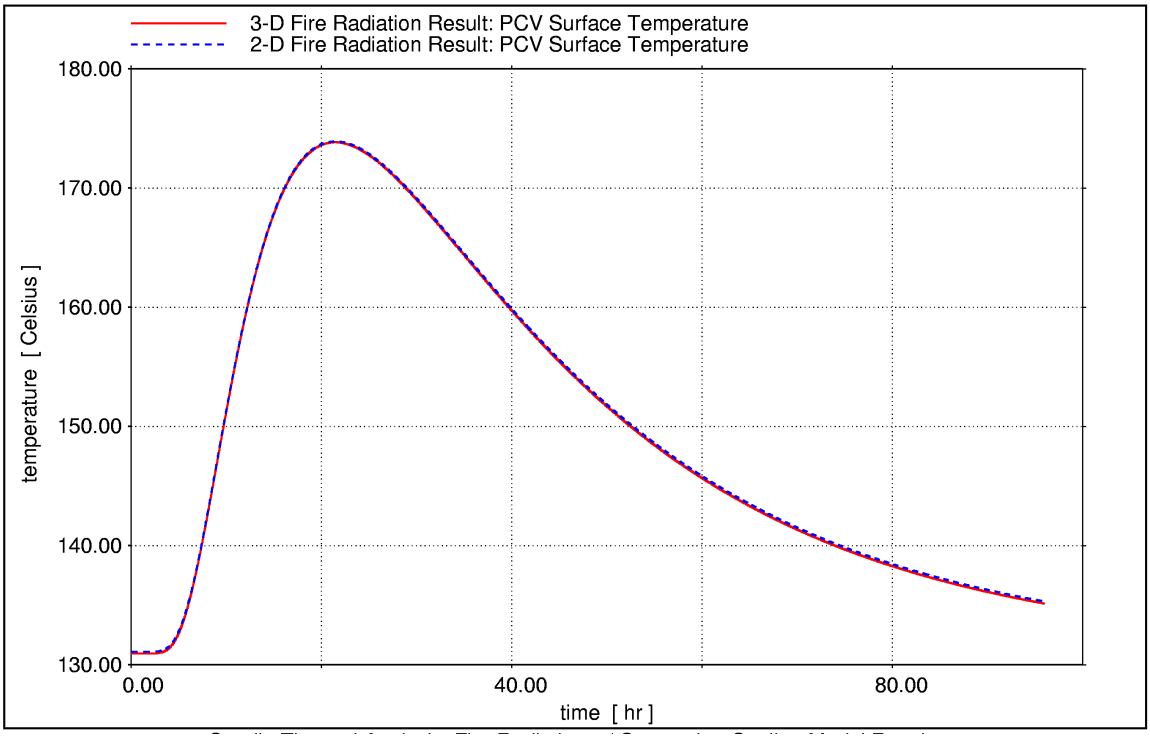

Figure 9b. Comparison of 2D Axisymmetric and 3D Model Simulations at Primary Containment Vessel Surface.

7. 3D End-on Impact Model

Figure 10a shows a photograph of the one-half scale test specimen following end-on impact as described in Bobbe and Pierce.[6] The impact occurred on the right side of the test specimen. Note that the end of the sectioned package (left side in the photograph) is missing. The deformed configuration was estimated based on this and other photos in Bobbe and Pierce.[6] The corresponding 3D finite element model is shown in Figure 10b. A 3D model was analyzed, though the deformed geometry is nearly axisymmetric. Note that fine details such as the buckling patterns on the outer shell and air gaps between components were not included in the thermal model. These details would not be reproducible from impact to impact and are not expected to significantly affect the thermal response.

Figure 11 shows the variation of temperature vs. time at the center of the primary containment vessel. Because of the high thermal conductivity of the steel and plutonium simulant, the temperature at all points on the primary containment vessel is roughly the same (i.e., within about 15°C). The temperature of the primary containment vessel initially decreases from its steady-state value because the material around it is crushed by the impact, resulting in increased thermal conductivity. This allows the hot center to transfer more heat to the cooler midwall regions of the container even though the outer wall is being heated by the external fire. The steady-state temperature long after the fire will differ from the initial steady-state value because of the changes in geometry and thermomechanical properties.

Figure 12 shows the temperature distribution at the end of the fire. The lowest temperatures are not necessarily at the center of the package because the internal power source causes heating. Figure 13 shows the temperature when the primary containment vessel reaches its peak – approximately 12 hours after the start of the fire.

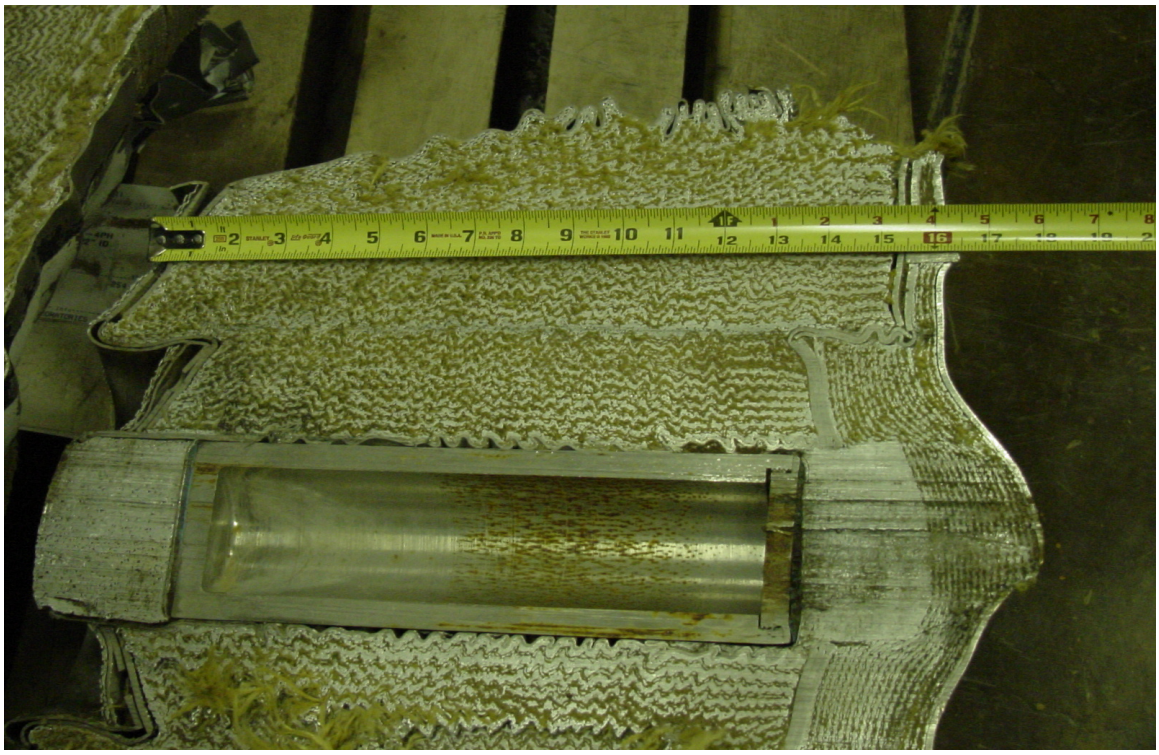

Figure 10a. Section View of One-half Scale PMATP after End-on Impact.

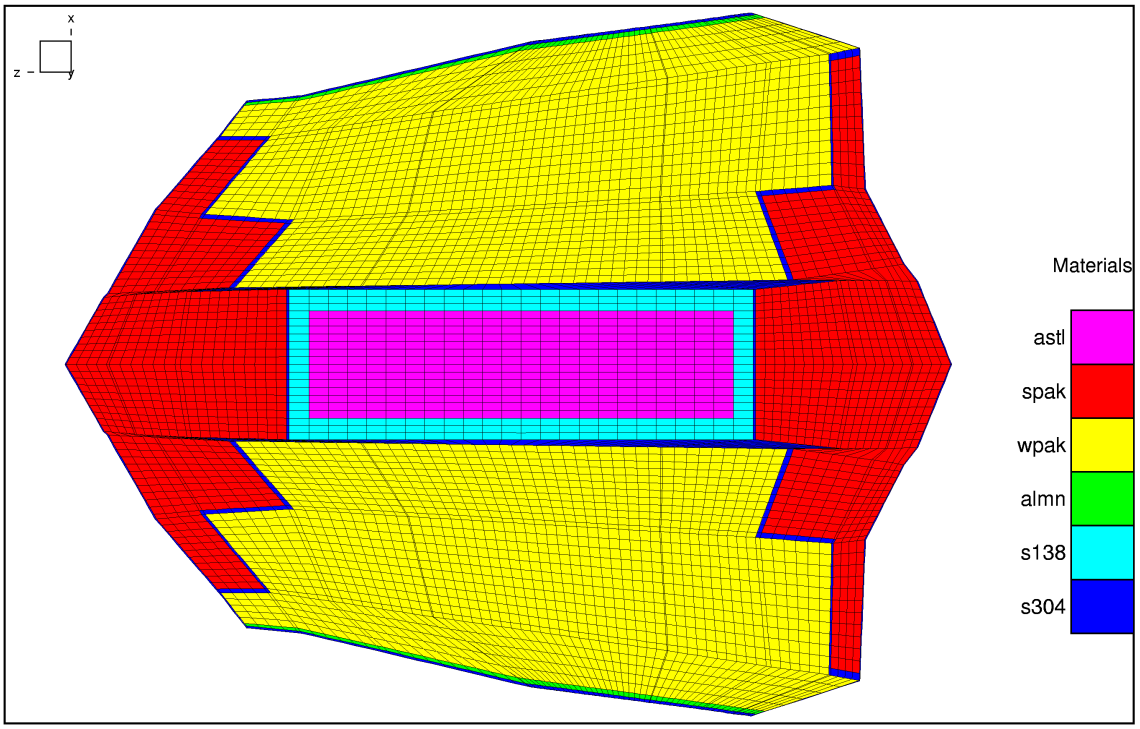

Figure 10b. Finite-element Model of PMATP after End-on Impact.

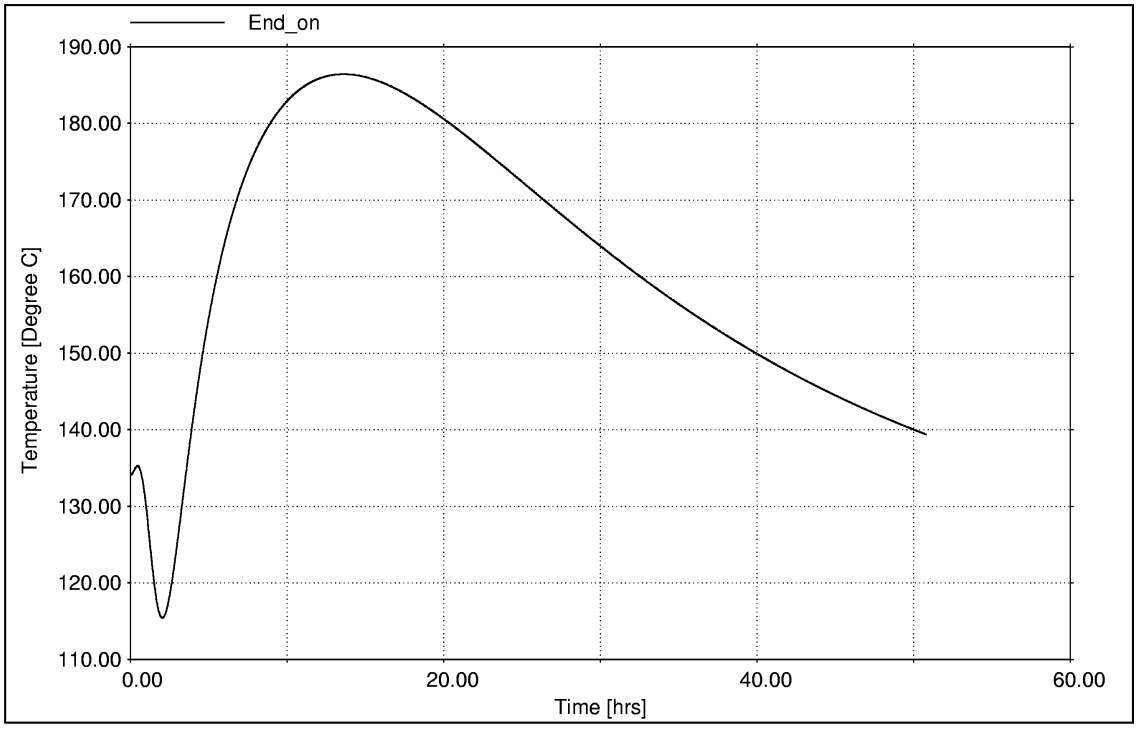

Figure 11. Temperature History at Center of Primary Containment Vessel After End-on Impact at Time 0.

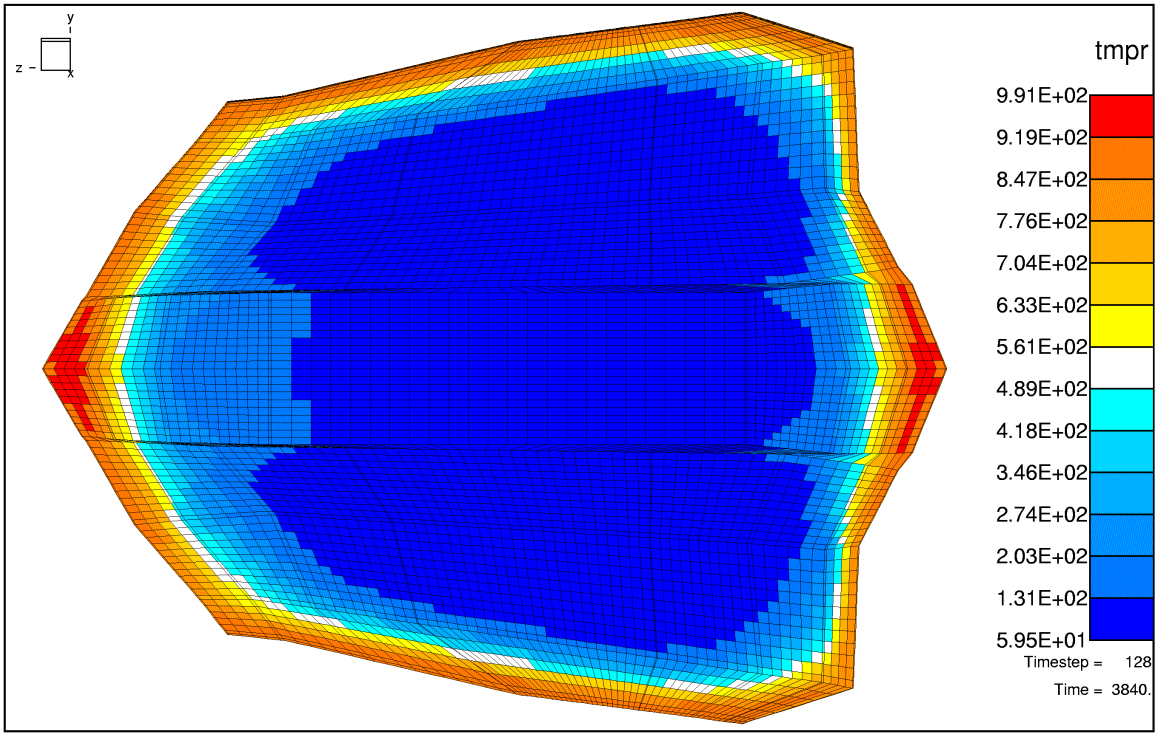

Figure 12. Temperature [°C] Distribution at End of Fire, End-on Impact.

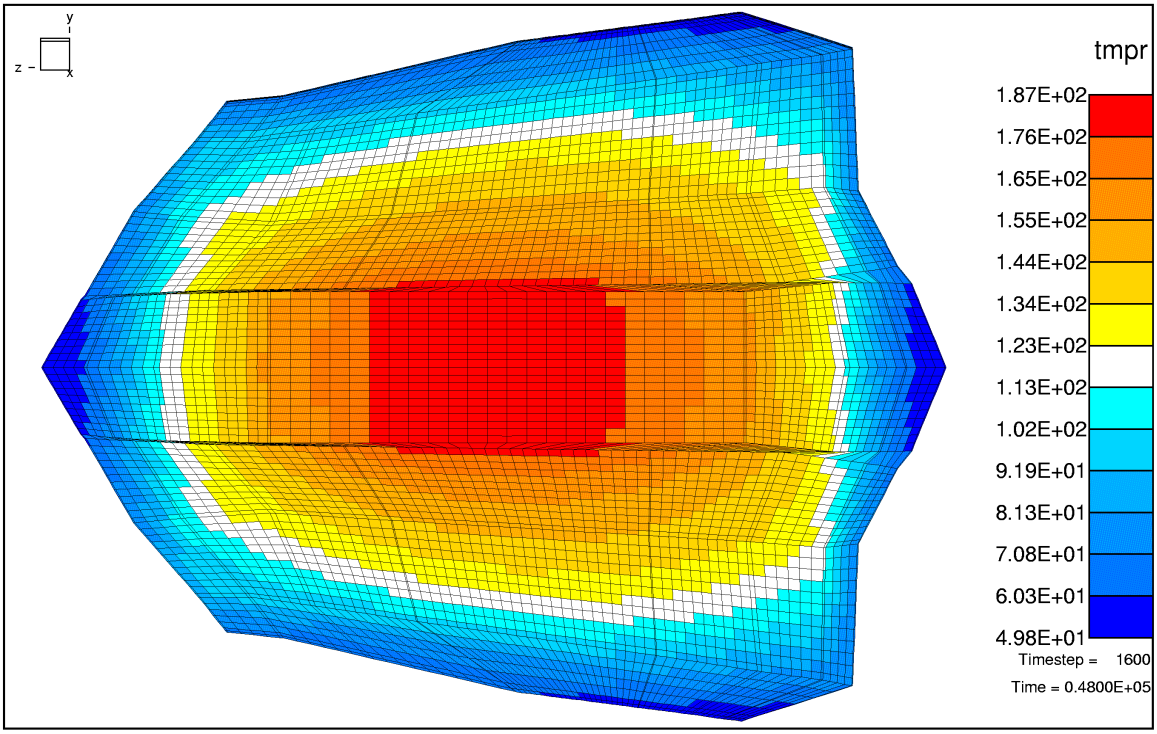

Figure 13. Temperature [°C] Distribution when Primary Containment Vessel is at its Peak Temperature (12 Hours After Start of Fire), End-on Impact.

8. 3D Side-on Impact Model

Figure 14a and Figure 14b show photographs of the one-half scale test specimen following side-on impact as described in Bobbe and Pierce.[6] The impact occurred on the left side of the photographs. The corresponding 3D finite element model is shown in Figure 15. Note that fine details such as the buckling patterns on the outer shell and air gaps between components were not included in the thermal model. These details would not be reproducible from impact to impact and are not expected to significantly affect the thermal response.

Figure 16 shows the variation of temperature vs. time at the center of the primary containment vessel when the deformed package is exposed to a one-hour 1000°C fire. Because of the high thermal conductivity of the steel and plutonium simulant, the temperature at all points on the primary containment vessel is roughly the same (i.e., within about 15°C).

Figure 17 shows the temperature distribution at the end of the fire. Figure 18 shows the temperature when the primary containment vessel reaches its peak value – approximately 12 hours after the start of the fire.

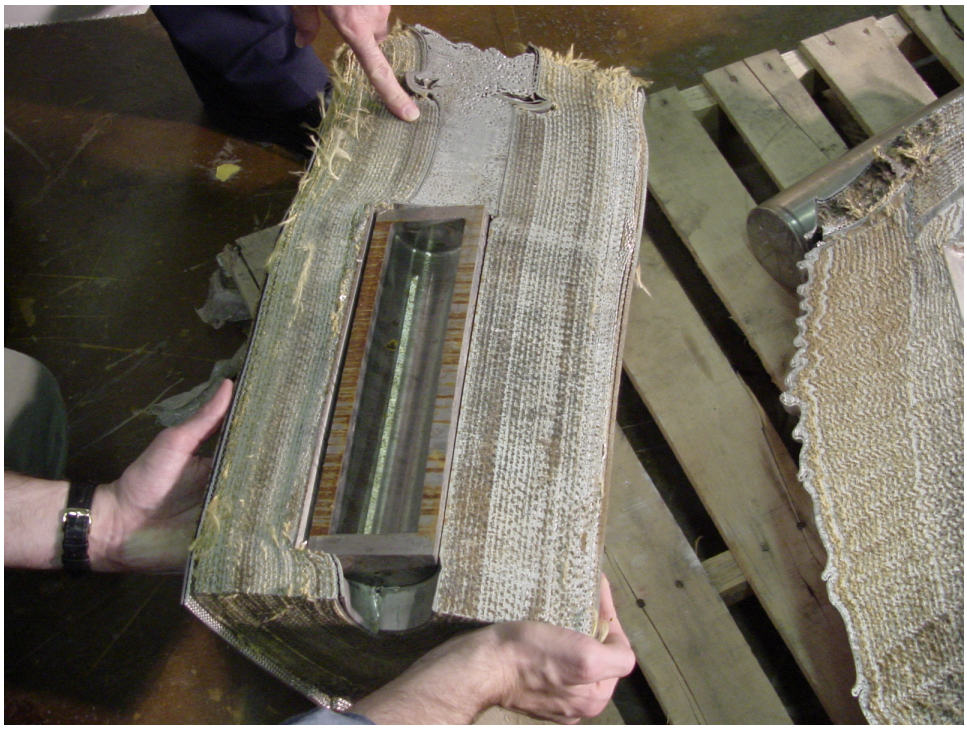

Figure 14a. Longitudinal Section of PMATP Following Side-on Impact.

Figure 14b. Transverse Section of PMATP Following Side-on Impact.

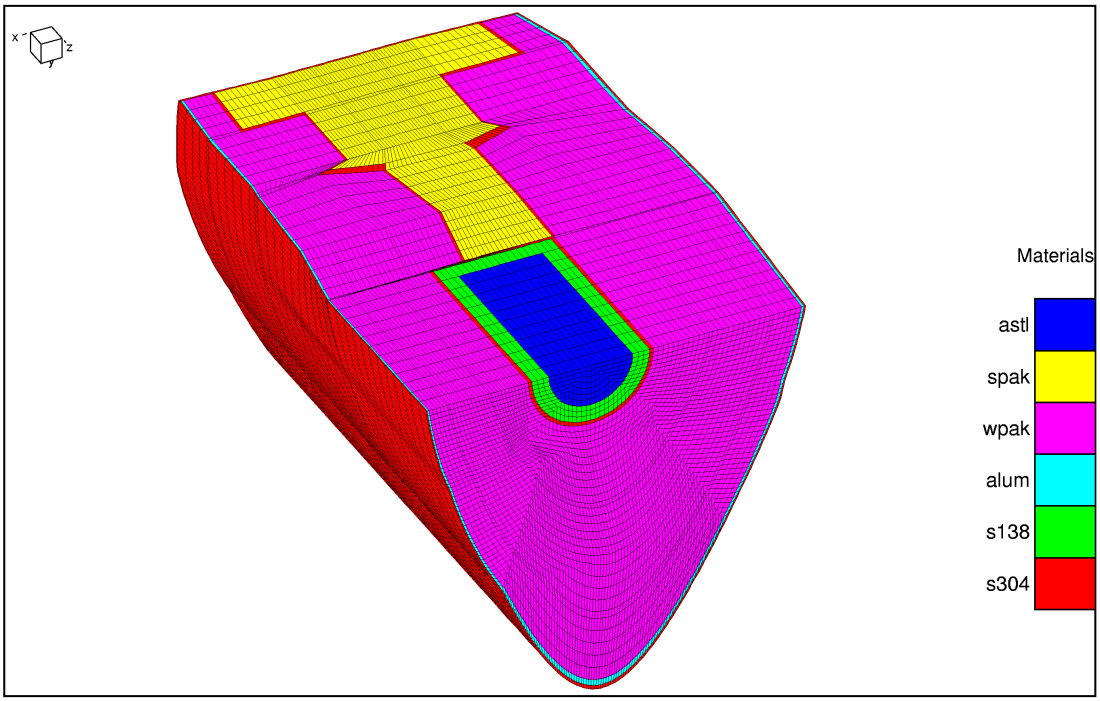

Figure 15. Sectioned Finite-element Model of PMATP Following Left Side (+x) Impact.

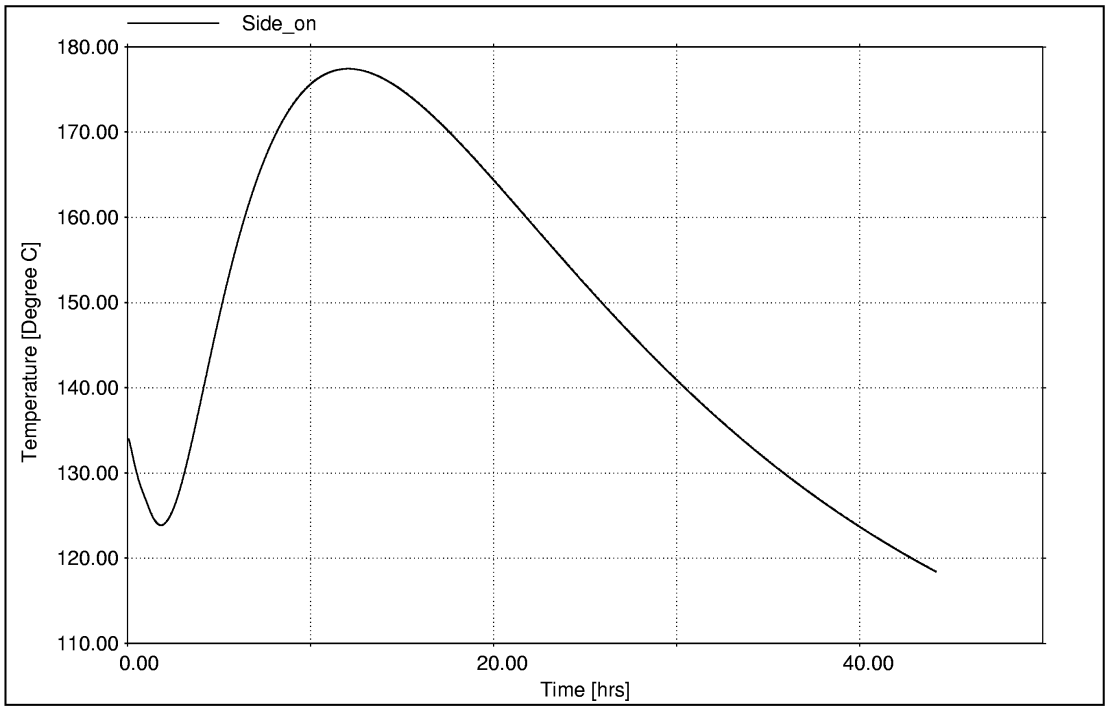

Figure 16. Temperature Variation vs. Time at Center of Primary Containment Vessel.

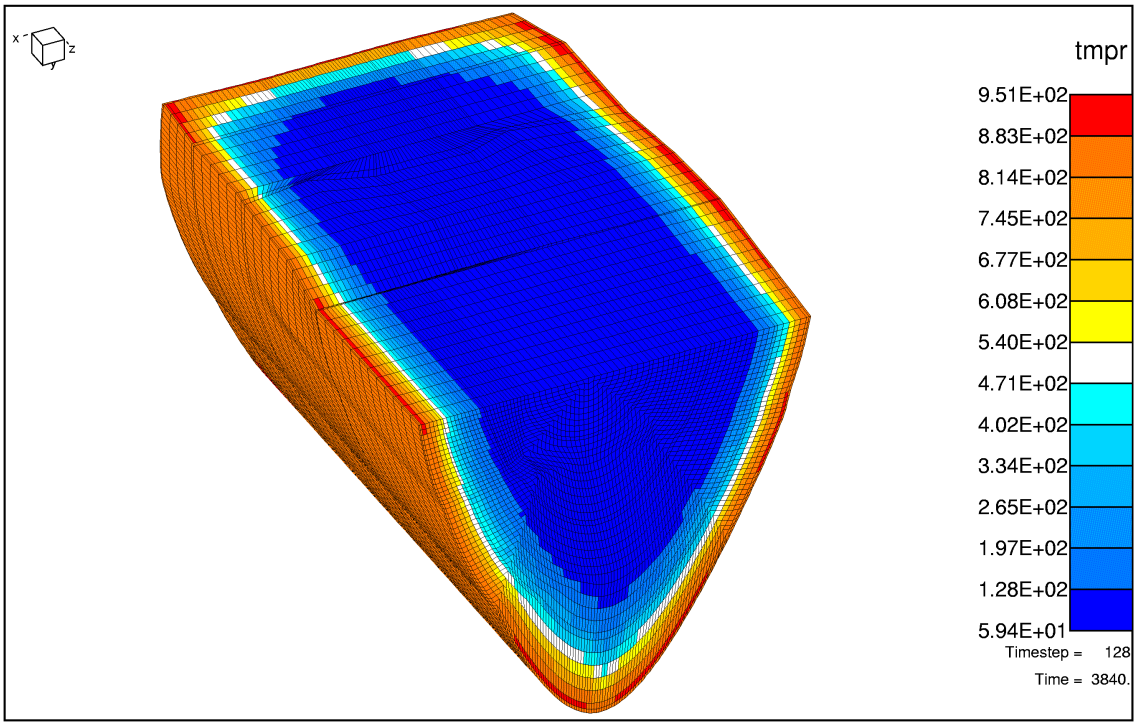

Figure 17. Temperature [°C] at End of Fire, Side-on Impact.

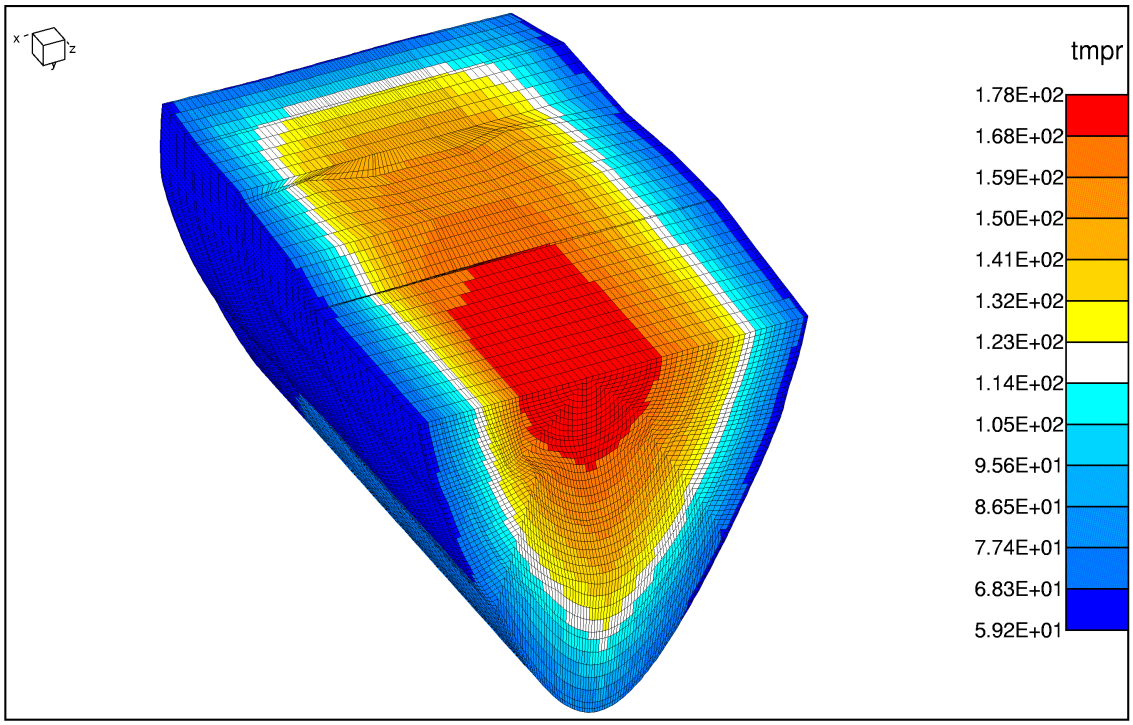

Figure 18. Temperature [°C] Distribution when Primary Containment Vessel is at its Peak Temperature (12 Hours After Start of Fire), Side-on Impact.

9. 3D Center-of-Gravity-Over-Corner Impact

Figure 19 shows a cross section of the one-half scale test specimen following center-of-gravity-over-corner impact as described in Lopez and Pierce.[5] The corresponding 3D finite element model is shown in Figure 20. The impact occurred on the lower left corner of the model. Note that fine details such as the buckling patterns on the outer shell and air gaps between components were not included in the thermal model. These details would not be reproducible from impact to impact and are not expected to significantly affect the thermal response.

Figure 21 shows the variation of temperature vs. time at the center of the primary containment vessel. Because of the high thermal conductivity of the steel and plutonium simulant, the temperature at all points on the primary containment vessel is roughly the same (i.e., within about 15°C).

Figure 22 shows the temperature distribution at the end of the fire. Figure 23 shows the temperature when the primary containment vessel reached its peak, which occurred approximately 22 hours after the start of the fire.

Figure 19. Cross Section of One-half Scale PMATP After CGOC Impact.

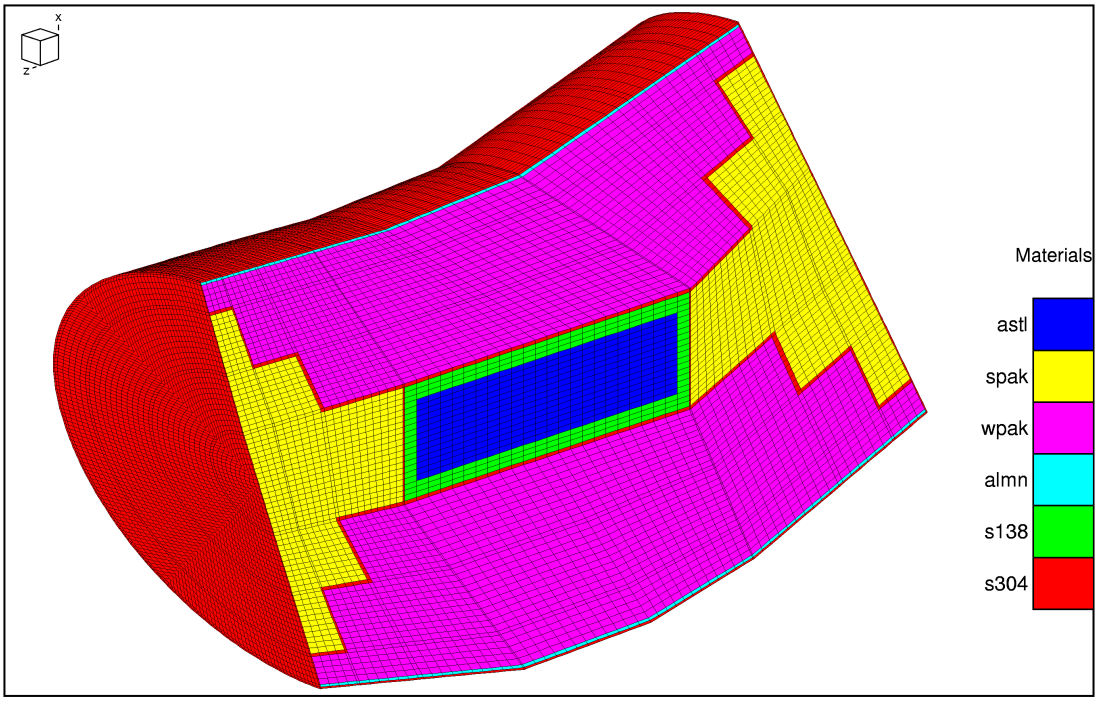

Figure 20. Finite-element Model of PMATP Following CGOC Impact.

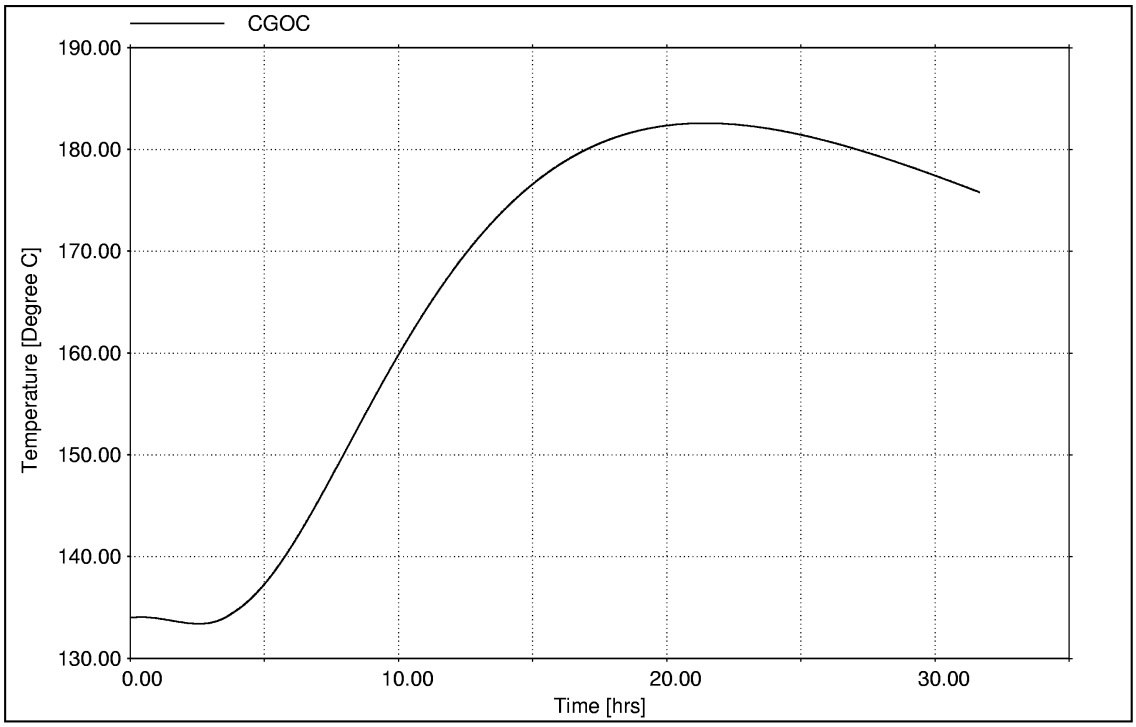

Figure 21. Temperature Variation vs. Time at Primary Containment Vessel Centroid, CGOC Impact.

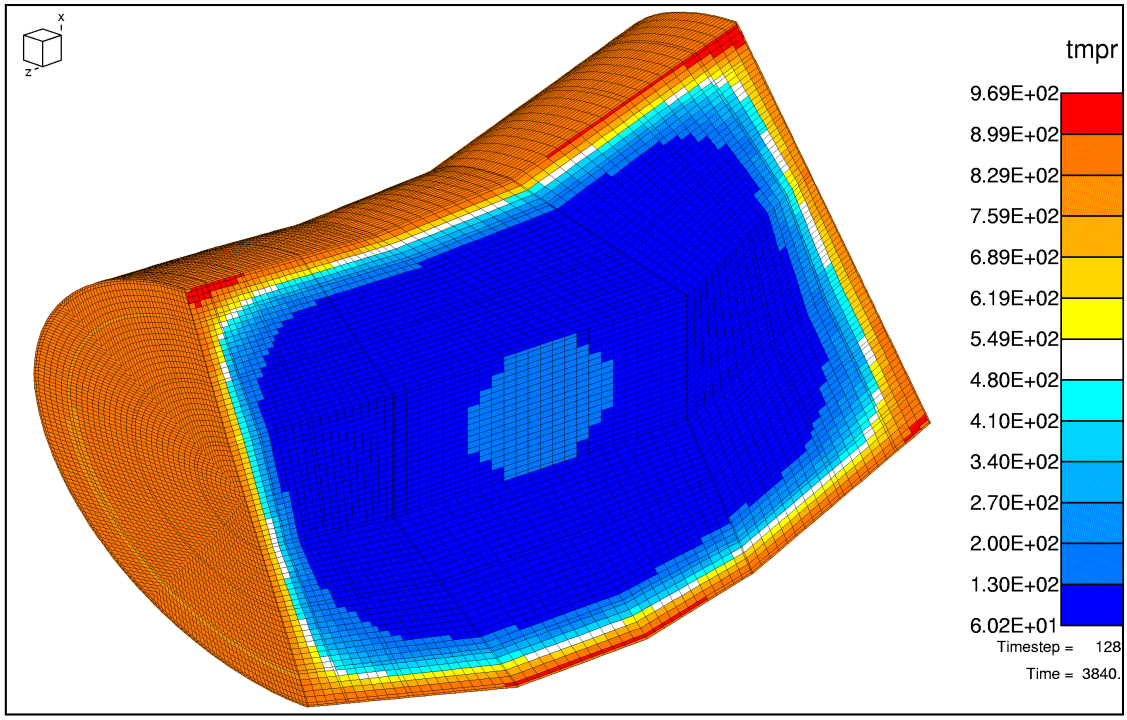

Figure 22. Temperature [°C] at End of Fire, CGOC Impact.

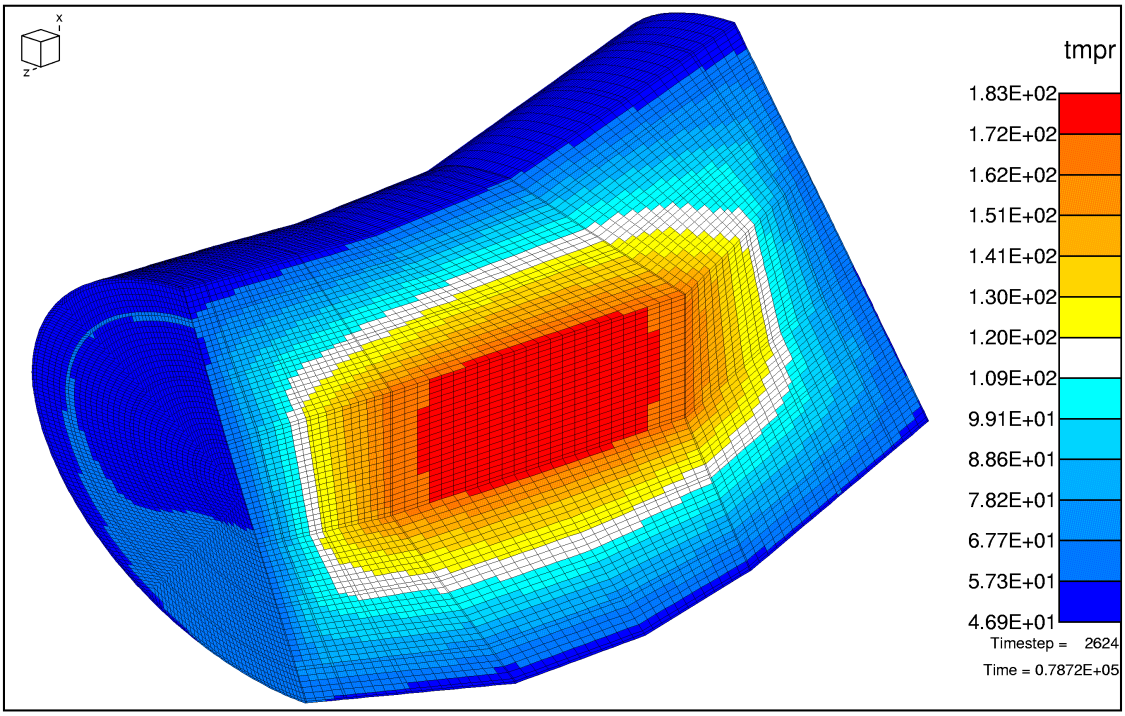

Figure 23. Temperature Distribution [°C] when Primary Containment Vessel is at its Peak Temperature (Approximately 22 Hours After Start of Fire), CGOC Impact.

10. Summary and Conclusions

Sandia National Laboratories has designed a crash resistant container (PMATP) for the air transport of plutonium capable of surviving a worst-case plane crash including both impact and subsequent fire. This report presents thermal analyses of the PMATP in its undamaged (pre-test) and in bounding post-accident states for side-on impact, end-on impact, and center-of-gravity over-corner (CGOC) impact. The goal of these thermal simulations was to evaluate the performance of the package in a worst-case post-crash fire.

Temperature distributions within the package are reported before impact, at the end of the fire, and at the times when peak primary containment vessel temperature was reached for the four impact cases considered. Figure 24 compares the time variation of temperature at the center of the primary containment vessel for the undeformed and for three of the post-impact states of the PMATP. For these analyses, the post-impact PMATP is assumed to be highly distorted, but intact. The analyses show that the post-impact states reach a higher peak temperature and reach it at an earlier time; however, the peak temperature increase is only about 10°C in the worst case. Though the thermal conductivity of the perforated aluminum increases dramatically in its crushed state, the overall insulating properties of the overpack material are dominated by the Kevlar®.

This analysis clearly predicts that the PMATP provides acceptable thermal response characteristics, both for the post-accident fire of a one-hour duration and the after-fire heat-soak condition. All predicted temperatures for the primary containment vessel are well within design limits for safety. The predictions, in fact, show that the temperatures would be well below the acceptable maximum working temperature of 230°C for most elastomers and far below the 1000°C limit for a high temperature braze or welded closure.

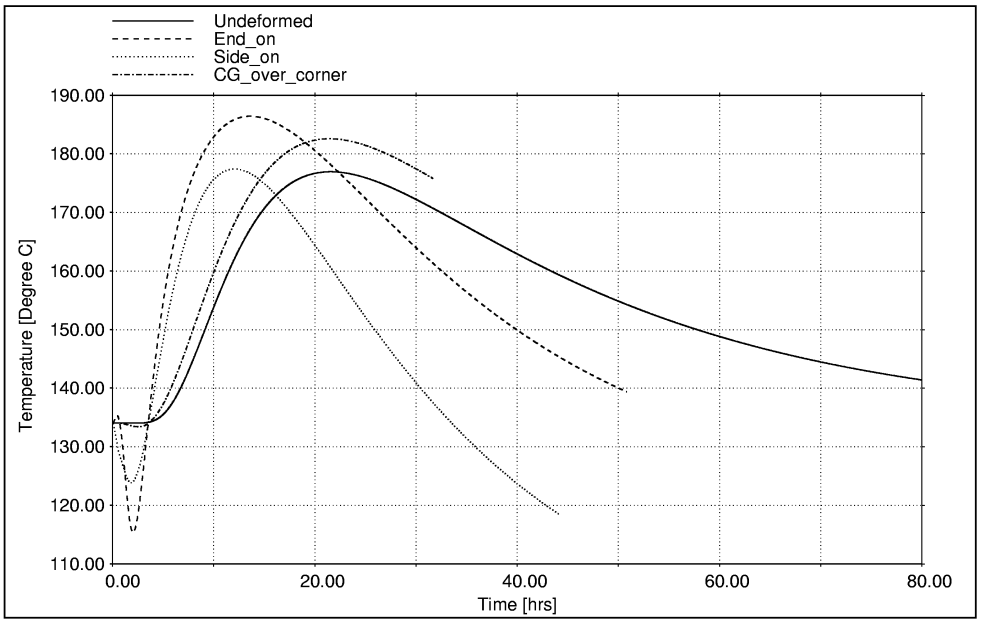

Figure 24. Time Variation of Temperature for the Undeformed and Deformed States of the PMATP at the Primary Containment Vessel Centroid.

This page intentionally left blank.

11. References

1. Pierce, J. D., U. S. Patent No. 5337917, *Crash Resistant Container*, August 16, 1994.

2. Vaughan, D. K., and J. Mould, *Flex User's Manual*, Version 1-J.6, Weidlinger Associates, Los Altos, California, 2000.

3. "Qualification Criteria to Certify A Package for Air Transport of Plutonium," NUREG-0360, U. S. Nuclear Regulatory Commission, Washington, DC, January 1978.

4. Todd, J. P. and H. B. Ellis, *Applied Heat Transfer*, Harper & Row, New York, New York, 1982.

5. Lopez, C. and J. D. Pierce, *Characterization of Thermophysical Properties of Perforated Aluminum and Aramid Cloth*, Procedures of the 13th International Symposium on the Packaging and Transportation of Radioactive Material, U. S. Dept. of Energy, Chicago, September 2001.

6. Bobbe, J. G. and J. D. Pierce, *Test Report for Perforated Metal Air Transportable Package (PMATP) Prototype*, SAND2003-2156, Sandia National Laboratories, Albuquerque, New Mexico, June 2003.

This page intentionally left blank.

DISTRIBUTION:

1 International Cooperation and Nuclear Material Management Division
Japan Nuclear Cycle Development Institute
4-49, Muramatsu, Tokai-Mura
Naka-Gun, Ibaraki, 319-1184 Japan
Attn : Mr. Tanaka Mitsuo, Director

13 Nuclear Material Management Section
International Cooperation and Nuclear Material Management Division
Japan Nuclear Cycle Development Institute
4-49, Muramatsu, Tokai-Mura
Naka-Gun, Ibaraki, 319-1184 Japan
Attn : Mr. Takafumi Kitamura, General Manager (1)
Mr. Yuichiro Ouchi, Packaging Safety (10)
Mr. Toro Ito, Packaging Safety (1)
Mr. Ken Shibata, Scientist (1)

1 Tokai Works, Plutonium Fuel Center
Technical Administration Division
Nuclear Material Management Section
Japan Nuclear Cycle Development Institute
4-33, Muramatsu, Tokai-Mura
Naka-Gun, Ibaraki, 319-1194 Japan
Attn : Mr. Kiyoaki Yamamoto, Senior Engineer

4 Nuclear Non-Proliferation & Safeguards Group
International Cooperation and Nuclear Material Management Division
Japan Nuclear Cycle Development Institute
4-49, Muramatsu, Tokai-Mura
Naka-Gun, Ibaraki, 319-1184 Japan
Attn : Mr. Keiichiro Hori, Group Leader (1)
Ms. Naoko Inoue, Assistant Senior Scientist (1)
Mr. Masayuki Usami, Assistant Senior Engineer (1)
Mr. J. P. Furaus, SNL on assignment to JNC (1)

3 Japan Nuclear Cycle Development Institute
Nuclear Emergency Assistance and Training Center
4-33, Muramatsu, Tokai-Mura
Naka-Gun, Ibaraki, 319-1184 Japan
Attn : Mr. Miyuki Igarashi, Group Leader (1)
Mr. Fumitaka Watanabe, System Operation Group (1)
Mr. Ryoji Yamanaka, Chief Senior Engineer (1)

1 Japan Nuclear Cycle Development Institute
Washington Office
1825 K Street, N.W.
Suite 508
Washington, D.C. 20006
Attn: Mr. Junichi Kurakami, Director

3 U.S. Department of Energy
Albuquerque Operations Office
PO Box 5400
Albuquerque, NM 87115
Attn: Mr. Gary Lanthrum (1)
Mr. Steven Hamp (1)
Mr. Ashok Kapoor (1)

13 Weidlinger Associates, Inc.
4410 El Camino Real
Suite 110
Los Altos, CA 94022
Attn: Mr. John Mould (10)
Mr. Howard Levine (1)
Mr. Robert Oneto (1)
Mr. Darren Tennant (1)

Sandia National Laboratories

1	MS0724	R. J. Eagan, 6000
1	MS0701	P. B. Davies, 6100
1	MS0701	F. Nimick, 6100
1	MS0718	K. B. Sorenson, 6141
1	MS0718	C. Lopez, 6141
1	MS0719	S. M. Howarth, 6142
50	MS0719	J. D. Pierce, 6142
5	MS0719	G. F. Hohnstreiter, 6142
1	MS0719	2134.000 File, 6142
2	MS0899	Technical Library, 9616
1	MS9018	Central Technical Files, 8945-1